Journal of Translational Medicine

RESEARCH

Open Access

Single-cell transcriptomic analysis deciphers the inflammatory microenvironment characterized by CXCL9+ fibroblasts and ACKR1+ endothelial cells in immune-related myocarditis

Boyu Sun[1,3†], Ziyu Xun[2†], Zixiang Zhou[2†], Nan Zhang[2], Mingjian Piao[2], Chengjie Li[2], Jiongyuan Li[2], Shuofeng Li[2], Longhao Zhang[2], Xiangqi Chen[2], Hanping Wang[1*] and Haitao Zhao[2*]

Abstract

Background Immune-related myocarditis induced by immune checkpoint inhibitors (ICIs) is a rare immune-related adverse event (irAE) but is characterized by a high mortality rate. However, the specific pathological mechanisms underlying immune-related myocarditis remain largely unclear. In this study, we aimed to elucidate the inflammatory microenvironment within cardiac tissues affected by immune-related myocarditis at the single-cell level to identify potential therapeutic targets.

Methods We performed single-cell RNA sequencing (scRNA-seq) on an endomyocardial biopsy specimen obtained from a patient with pancreatic neuroendocrine carcinoma who developed immune-related myocarditis following treatment with ICIs. Additionally, the scRNA-seq data of heart specimens from deceased donors without cardiovascular diseases were collected and applied as normal control. To validate our findings and assess their specificity to ICI-related pathology, we analyzed mouse scRNA-seq data, including controls, ICI-related myocarditis, viral myocarditis, and autoimmune myocarditis.

Results We found elevated proportions of lymphocytes, myeloid cells, and fibroblasts in the irAE group, suggesting an intensified inflammatory microenvironment in human immune-related myocarditis. Within the lymphocyte compartment, increased proportions of CD8 + T exhausted cells and CD8 + T proliferative cells were observed in the irAE group. The upregulated differentially expressed genes in myeloid cells in the irAE group were enriched in pro-inflammatory pathways, consistent with the observed metabolic shift from oxidative phosphorylation to glycolysis.

†Boyu Sun, Ziyu Xun and Zixiang Zhou contributed equally to this work and shared first authorship.

*Correspondence:
Hanping Wang
wanghanping78@163.com
Haitao Zhao
zhaoht@pumch.cn

Full list of author information is available at the end of the article

CXCL9 + fibroblasts, characterized by the production of multiple pro-inflammatory cytokines and enriched in the JAK-STAT and TNFα signaling pathways, were predominantly found in the irAE group. Venous endothelial cells specifically expressing atypical chemokine receptor-1 (*ACKR1*) interacted with myeloid cells and CXCL9 + fibroblasts through the CXCL signaling pathway, facilitating chemokine transcytosis and leukocyte recruitment. Analysis of murine scRNA-seq data further supported these findings, revealing that exhausted CD8 + T cells and pro-inflammatory fibroblasts were uniquely enriched in ICI-related myocarditis, reflecting its distinct inflammatory microenvironment.

Conclusions We elucidated the unique inflammatory microenvironment of immune-related myocarditis at the single-cell level. Our work revealed key cell subpopulations that were significantly implicated in inflammation, thus offering potential therapeutic targets.

Keywords Immune checkpoint inhibitor, Immune-related myocarditis, Single-cell RNA sequencing, Intercellular communication, Inflammatory microenvironment

Background

Immunotherapy has profoundly transformed the paradigm of cancer treatment in the past decade. Immune checkpoint inhibitors (ICIs) mainly target programmed cell death 1 (PD-1) or programmed cell death 1 ligand 1 (PD-L1) and cytotoxic T lymphocyte-associated protein 4 (CTLA-4), releasing T cells from the inhibition by cancer cells and thus enhancing their cytotoxicity. While the application of ICIs has yielded substantial survival benefits for patients across diverse cancer types, it also comes with the potential for various immune-related adverse events (irAEs) affecting multiple organs and tissues throughout the body [1]. Severe irAEs can interrupt anti-tumor therapy, compromise organ function, and even pose life-threatening risks. Myocarditis is a rare irAE but has a high mortality rate ranging from 25 to 50% in patients receiving ICIs [2]. Mechanistically, immune-related myocarditis is characterized by the infiltration of T cells and macrophages into heart tissues, leading to localized inflammation and cardiomyocyte damage [3]. However, the more specific mechanisms of immune-related myocarditis have not yet been fully elucidated. Corticosteroids are the first-line therapy recommended for immune-related myocarditis, with additional treatments such as immunosuppressive agents, intravenous immunoglobulin, and plasmapheresis being utilized in some complicated cases [4]. Nevertheless, some patients exhibit poor responses to treatment, indicating the need for further exploration into the complex microenvironment of immune-related myocarditis. Moreover, ICI-related myocarditis may exhibit distinct inflammatory and immunopathological features compared to myocarditis caused by other etiologies, such as viral infections, autoimmunity, or toxin exposure [5].

The emergence of single-cell technologies, exemplified by single-cell RNA sequencing (scRNA-seq), has encouraged researchers to elucidate the characteristics of individual cells within tissues. Several studies have leveraged single-cell technologies to decipher the cellular landscape of heart tissues affected by immune-related myocarditis in mice. Zhu et al. reported an expansion of effector memory CD8 + T cells in the heart tissues of $Pdcd1^{-/-}$ mice with spontaneous myocarditis compared with those of controls [6]. Axelrod et al. revealed that effector CD8 + T cells present in the hearts of $Pdcd1^{-/-}$ $Ctla4^{+/-}$ mice were specific for α-myosin and that depletion of CD8 + T cells could attenuate myocarditis [7]. Ma et al. discovered that in $Ctla4^{+/-}$ $Pdcd1^{-/-}$ ICI myocarditis mice, CXCL9 + CXCL10 + macrophages interacted with CD4 + and CD8 + T cells through the interferon (IFN)-γ signaling pathway [8]. Blockade of IFN-γ signaling was shown to reduce the expansion of CXCL9 + CXCL10 + macrophages and ameliorate myocarditis. These studies primarily concentrated on T cells and macrophages infiltrating heart tissues in mice, yet they lacked investigations into stromal cells, which constitute a significantly higher proportion and may also contribute to immune-related myocarditis in humans.

In this study, we conducted scRNA-seq on the endomyocardial biopsy sample obtained from a patient diagnosed with immune-related myocarditis. Additionally, we utilized scRNA-seq data of normal heart tissues obtained from donated specimens as controls [9], aiming to compare the cellular composition and functional differences between immune-related myocarditis and normal cardiac tissues. We identified crucial subpopulations of T/natural killer (NK) cells, myeloid cells, endothelial cells, and fibroblasts, which might contribute to myocardial inflammation and represent potential therapeutic targets. To validate our findings, we compared immune-related myocarditis with controls using mouse scRNA-seq data and further contrasted it with viral and autoimmune types, highlighting the unique inflammatory features of immune-related myocarditis.

Methods

Patient information and sample collection

A 71-year-old male with stage IV pancreatic neuroendocrine carcinoma (T4NxM1) and a PD-L1 tumor proportion score (TPS) of 30% received combination therapy of

lenvatinib (8 mg/day) and toripalimab (a PD-1 inhibitor, 240 mg every three weeks). Eighteen days after the initiation of immunotherapy, he developed precordial discomfort and intermittent chest pain. Laboratory tests revealed markedly elevated cardiac biomarkers, including creatine kinase (CK: 959 U/L), creatine kinase-MB (CK-MB: 35 μg/L), and cardiac troponin I (cTnI: 0.19 μg/L), raising clinical suspicion of immune-related myocarditis. Cardiac magnetic resonance imaging revealed linear mid-wall late gadolinium enhancement in the basal interventricular septum, with no abnormalities on T2-weighted imaging. Endomyocardial biopsy was performed for immunohistochemistry and scRNA-seq to confirm the diagnosis of immune-related myocarditis. Biopsies were taken from the right side of the interventricular septum. This study was approved by the Ethics Committee of Peking Union Medical College Hospital. Written informed consent was provided by the patient.

scRNA-seq data acquisition and generation

The endomyocardial biopsy sample was washed in ice-cold RPMI1640 medium and dissociated using Multi-tissue dissociation kit 2 (Miltenyi). The number and viability of cells were determined by a fluorescence cell analyzer (Countstar® Rigel S2) with acridine orange (AO)/propidium iodide (PI) reagent after removing erythrocytes (Miltenyi 130-094-183). Then debris and dead cells were removed (Miltenyi 130-109-398/130-090-101). Finally, cells were washed twice in the RPMI1640 and resuspended in 1×phosphate-buffered saline (PBS) containing 0.04% bovine serum albumin at a concentration of 1×10^6 cells/mL. The scRNA-seq libraries were constructed using a SeekOne® MM Single Cell 3' Library Preparation Kit following the manufacturer's instructions (SeekGene, Beijing, China). The indexed sequencing libraries were cleaned with SPRI beads and sequenced on the Illumina NovaSeq 6000 platform with PE150 read length.

The raw scRNA-seq data of normal hearts were downloaded from the Human Cell Atlas (ERP123138) [9]. Heart samples were obtained from deceased donors without a history of cardiovascular disease. Four normal heart tissue samples, including two right verticle (RV) samples and two interventricular septum (SP) samples, were included in our study as normal controls. The raw data were then mapped to the reference genome GRCh38-3.0.0 with the CellRanger (v3.1.0) provided by 10× Genomics. Downstream bioinformatic analysis was carried out using R software (v4.3.1). The clinical information and sample details were summarized in Additional file 1: Table S1.

scRNA-seq data processing

The R package Seurat (v4.3.0.1) was applied to analyze the scRNA-seq data [10]. A total of 19,121 cells from five samples were integrated and used for downstream analysis. For quality control, cells with 200 ≤ gene numbers (nFeature_RNA) ≤ 3500, mitochondrial gene percentage ≤ 20%, and ribosomal gene percentage ≤ 20% were retained. Potential doublets were detected using the Python package Scrublet (v0.2.3) [11], and cells with doublet scores > 0.3 were excluded. Ambient RNA contamination was assessed using the R package DecontX (v1.4.0) [12], and cells with contamination scores > 0.15 were removed. A total of 15,639 high-quality cells passed the quality control filtering and were utilized for subsequent analysis. The single-cell count data matrix was normalized using the "NormalizeData" function. The top 2000 highly variable features were selected for principal component analysis (PCA) dimensionality reduction via the "RunPCA" function. For batch correction, we applied the "RunHarmony" function in the R package harmony (v0.1.1) to integrate different samples and eliminate the technical batch variations across patients [13]. Then we used "FindNeighbors" and "FindClusters" to cluster the cells. The R package clustree (v0.5.0) was applied to show the relationships between clusters and determine the clustering resolution [14]. "RunUMAP" and "RunTSNE" were used to visualize the dimension reduction plots of cells.

Cell type annotation

We identified the marker genes of each cluster by running the "FindAllMarkers" algorithm and annotated the clusters manually based on the expression of cell-specific genes reported in previous studies. We first grouped cells into seven major clusters, including lymphocytes (*NKG7*, *TRBC2*, and *CD3D*) [15], myeloid cells (*S100A8*, *S100A9*, and *LYZ*) [16], fibroblasts (*DCN*, *COL1A1*, and *GSN*) [9, 17], endothelial cells (*VWF*, *CLDN5*, and *PECAM1*) [9, 18], pericytes (*AGT*, *RGS5*, and *ABCC9*) [9, 19], smooth muscle cells (*TAGLN*, *MYH11*, and *TPM2*) [9, 20], and neuronal cells (*PLP1*, *NRXN1*, and *S100B*) [9, 18]. To delve deeper into the subclusters of these major cell types, we reclustered lymphocytes, myeloid cells, fibroblasts, and endothelial cells by repeating the aforementioned steps. Endothelial cell (EC) subpopulations were annotated based on reported marker genes: arterial ECs (*ARL15*, *HEY1*, *SEMA3G*, and *IGFBP3*) [9, 21], capillary ECs (*FCN3*, *RGCC*, and *CA4*) [9, 21], venous ECs (*VCAM1*, *PLVAP*, and *ACKR1*) [9, 22], and lymphatic ECs (*TBX1*, *PROX1*, *CCL21*, and *MMRN1*) [9, 21, 23].

Gene enrichment analysis

To investigate the differences in pathway enrichment between two clusters or two groups, differentially expressed genes (DEGs) were first identified with "FindAllMarkers" or "FindMarkers" in Seurat. Genes with $|\text{avg\_log}_2\text{FC}| > 0.5$ and adjusted p-values < 0.05 were

considered as significant DEGs and were selected for enrichment analysis. Then the R package clusterProfiler (v4.11.0) was used to perform Gene Ontology (GO) and Kyoto Encyclopedia of Genes and Genomes (KEGG) pathway analyses on selected DEGs with "enrichGO" and "enrichKEGG" [24]. Enriched pathway items with adjusted p-values < 0.05 were considered to be functionally significant. Gene set enrichment analysis (GSEA) was performed by "gseGO" and "GSEA" in clusterProfiler. Hallmark gene sets used in GSEA were downloaded from the MSigDB database (https://www.gsea-msigdb.org/gsea/msigdb).

Gene set variation analysis

Gene set variation analysis (GSVA) was performed with the R package GSVA (v1.42.0) [25]. Hallmark (H), curated (C2), and ontology (C5) gene sets were downloaded from the MSigDB database. The signature gene sets of T cells were based on previous studies [26, 27], including naive signature (*CCR7*, *LEF1*, *SELL*, and *TCF7*), regulatory signature (*IL2RA*, *IL4R*, *IL7*, *TGFB1*, *TGFB3*, *TGFBI*, and *TGFBR1*), costimulatory signature (*CD226*, *ICOS*, *SLAMF1*, *TNFRSF14*, *TNFRSF25*, and *TNFRSF9*), cytotoxic signature (*CST7*, *GZMA*, *GZMB*, *IFNG*, *NKG7*, and *PRF1*), exhausted signature (*BTLA*, *CTLA4*, *HAVCR2*, *LAG3*, *PDCD1*, and *TIGIT*), and proliferative signature (*STMN1* and *TUBB*). The metabolic signature gene sets were downloaded from a curated database [28].

Signature score calculation

To evaluate the inflammatory signatures of subsets of monocytes/macrophages in the irAE and normal groups, we calculated the signature scores of CD14 + monocytes, CD16 + monocytes, antigen-presenting macrophages, and LYVE1 + macrophages in the irAE and normal groups. The M1, M2, pro-inflammatory, and anti-inflammatory signature gene sets were obtained from previous studies [29, 30] and were listed in Additional file 1: Table S2. The enrichment score of each cell was calculated using "AddModuleScore" in Seurat.

Developmental trajectory analysis

To construct single-cell developmental trajectories of monocytes/macrophages, we adopted the R package monocle3 (v1.2.9) to calculate the pseudotime values of single cells [31]. We set the parameter num_dim = 100 in "preprocess_cds" and reduction_method="UMAP" in "reduce_dimension" and "plot_cells". In addition, "learn_graph" was used to establish the trajectory. We set CD14 + monocytes as the root of trajectory in "order_cells" based on previous literature indicating that CD14 + monocytes might be the precursors of monocytes/macrophages. The function "graph_test" was adopted to identify genes that were differentially expressed along the trajectory, and the alterations in gene expression were displayed in the form of heatmaps. The monocle2 algorithm (v2.30.0) was also applied to construct a differentiation tree for monocytes/macrophages using the DDRTree method with default parameters [32].

Cell-cell communication analysis

The R package CellChat (v1.6.1) was applied to infer the ligand-receptor interactions among different cell clusters [33]. The normalized gene expression matrix of cells was used as input data. The visualization of cell-cell communication results was also achieved by CellChat. To compare the intercellular communication networks between immune-related myocarditis and normal heart tissue, we ran CellChat on gene expression matrices of the irAE group and normal group separately and merged them by the "mergeCellChat" function. Ligand-receptor interactions with p-values < 0.05 were considered significant.

Pathway analysis and transcription factor analysis

The R package decoupleR (v2.8.0), which facilitates access to the PROGENy model and DoRothEA gene regulatory network, was applied to calculate the biological activities of single cells based on the normalized log-transformed gene expression matrix [34]. The PROGENy model contains signature genes of 14 canonical pathways and was used to calculate the pathway activity scores of each cell. The DoRothEA network is a database containing information on the interactions between transcription factors and their targets and was used to predict the transcription factor activities of each cell.

Cytokine signaling analysis

We utilized the CytoSig platform (https://cytosig.ccr.cancer.gov/) to predict cytokine signaling activities of different cellular clusters [35]. We generated the scaled gene expression matrix of four fibroblast subclusters using the "AverageExpression" function in Seurat and used it as input data for CytoSig. Then we downloaded the cytokine activity prediction results and employed them for subsequent analysis and visualization in R.

Analysis of murine scRNA-seq data

To validate findings in humans and compare immune-related myocarditis with other myocarditis subtypes, we analyzed five publicly available mouse scRNA-seq datasets from the Gene Expression Omnibus database: GSE213486 [7] and GSE227437 [8] for ICI-related myocarditis; GSE174458 [36] and GSE189636 [37] for viral myocarditis; and GSE142564 [38] for autoimmune myocarditis (Additional file 1: Table S5). Corresponding control samples were used as references for downstream comparisons. The canonical correlation analysis (CCA) method was applied to correct for batch effects in mouse

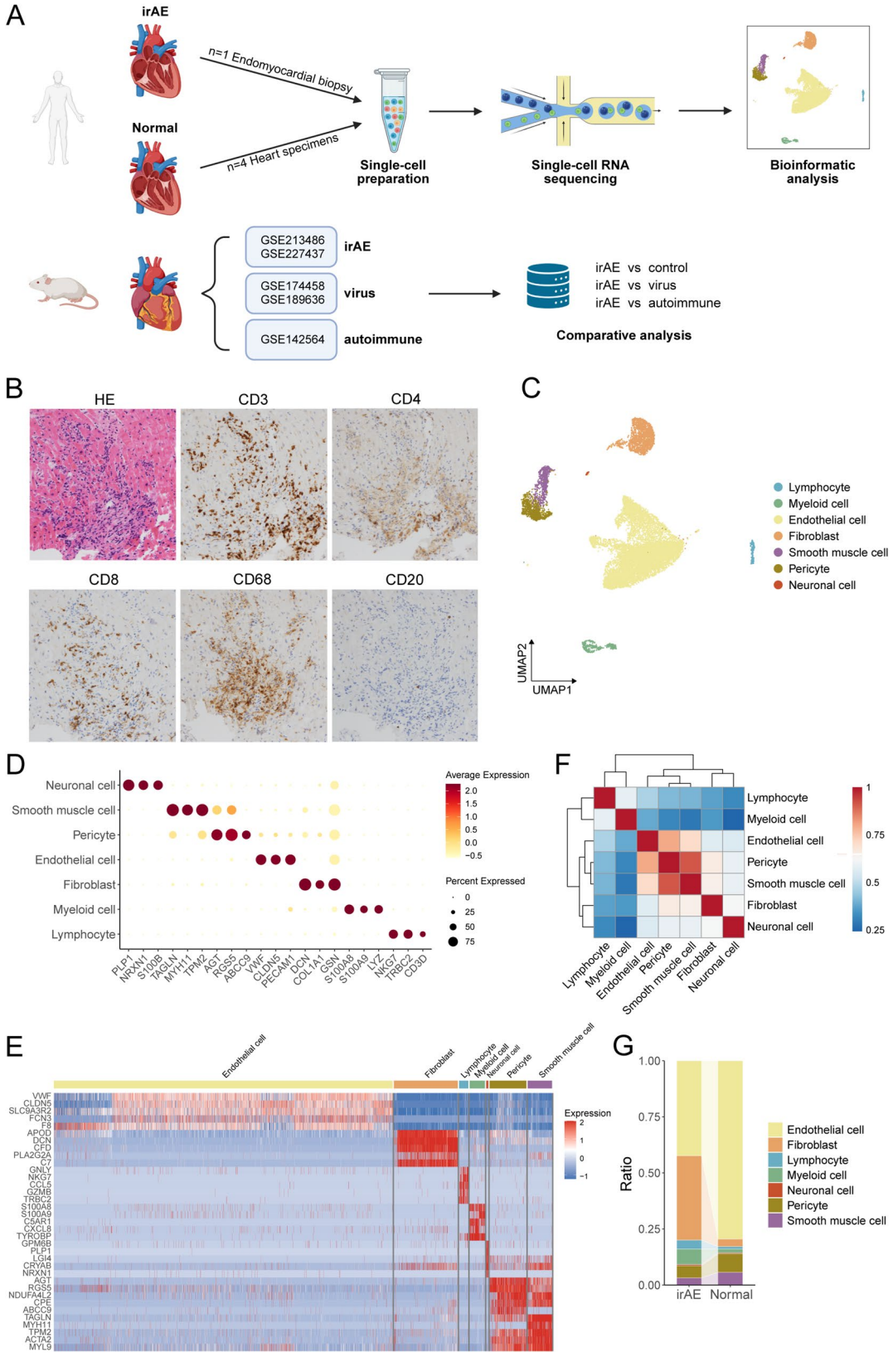

Fig. 1 (See legend on next page.)

(See figure on previous page.)

Fig. 1 Single-cell landscape of immune and stromal cells of heart tissues. (**A**) Workflow of the overall study design. Created with *BioRender.com*. (**B**) Hematoxylin-eosin (**H**&**E**) staining and immunohistochemistry (IHC) staining (positive for CD3, CD4, CD8, and CD63; negative for CD20) of endomyocardial biopsies from the patient diagnosed with immune-related myocarditis (150× magnification). (**C**) Uniform Manifold Approximation and Projection (UMAP) projection of all captured cells which are colored by major cell types. (**D**) Dot plot showing the expression of marker genes of seven major cell types. The dot size and color indicate the percentage and level of expression, respectively. (**E**) Heatmap of the top 5 differentially expressed genes (DEGs) expression of each major cell cluster. (**F**) Cell type correlation heatmap showing the relationship among seven major cell subpopulations based on the average expression of the top 2,000 variable genes ranked by standard deviation, using Spearman's correlation analysis. (**G**) Proportions of major cell types in the irAE and normal groups. irAE, immune-related adverse event

data [39]. The cell distribution variance of each cell subset across different pathogenic groups was assessed by calculating the ratio of observed to expected (Ro/e) cell numbers [40]. An Ro/e score greater than 1 indicated enrichment of the particular cell cluster in the corresponding group.

Statistical analysis

All statistical analyses and presentations were performed in R. All statistical tests used were defined in the figure legends. Statistical significance was set at p-value or adjusted p-value < 0.05.

Results

Single-cell characterization of the immune-related myocarditis microenvironment

To explore the mechanisms underlying immune-related myocarditis, we performed scRNA-seq on the endomyocardial biopsy obtained from a patient who received the anti-PD-1 inhibitor toripalimab and was pathologically confirmed to have immune-related myocarditis (Fig. 1A, B). Moreover, we collected scRNA-seq data from 4 heart samples obtained from deceased donors to serve as normal controls, aiming to elucidate the differences between the irAE group and the normal group (Fig. 1A).

After stringent quality control, a total of 15,639 single cells were obtained from irAE and normal heart tissues. Cardiomyocytes were excluded as they were difficult to capture by droplet-based scRNA-seq technology [41] and all other cells were included in the subsequent analysis. The cells were clustered into seven major cell types, including lymphocytes, myeloid cells, endothelial cells, fibroblasts, smooth muscle cells, pericytes, and neuronal cells (Fig. 1C; Additional file 2: Fig. S1A). The clusters were identified based on the expression of canonical cell markers (Fig. 1D, E; Additional file 2: Fig. S1B). Non-immune cells dominated heart tissues, while immune cells, including lymphocytes and myeloid cells, were scarce. The cell type correlation matrix also revealed a distinct separation of phenotypes between immune cells and non-immune cells, with stronger correlations observed among endothelial cells, pericytes, and smooth muscle cells, which were associated with the cardiac vasculature (Fig. 1F). Compared with normal heart tissues, the heart with immune-related myocarditis had an increased proportion of immune cells, consistent with the fact that a large number of immune cells were recruited to the heart in myocarditis (Fig. 1G). This pattern was consistent across all the samples (Additional file 2: Fig. S1C). Notably, fibroblasts were significantly more abundant in the irAE group, indicating that damaged myocytes were gradually substituted by fibroblasts when the inflamed heart tissue healed [42].

CD8 + T cells were converted to an exhausted state in immune-related myocarditis

To gain a deeper understanding of the T/NK compartment, we identified 5 subsets of lymphocytes, including CD4 + T, CD8 + effector memory T (CD8 + Tem), CD8 + exhausted T (CD8 + Tex), CD8 + proliferative T (CD8 + Tprolif), and NK cells (Fig. 2A; Additional file 2: Fig. S2A). Among the subpopulations of CD8 + T cells, CD8 + Tem cells highly expressed the cytotoxic marker *GZMA* and the effector memory marker *GZMK* (Fig. 2B) [43]. CD8 + Tex cells expressed high levels of immune checkpoint genes *CTLA4*, *HAVCR2*, *LAG3*, and *TIGIT* (Additional file 2: Fig. S2B, C), representing an exhausted state. CD8 + Tprolif cells exhibited specific expression of proliferative markers *MKI67*, *STMN1*, and *TOP2A* (Fig. 2B; Additional file 2: Fig. S2B, C). Utilizing canonical gene signatures of T cell subtypes, we observed that CD8 + Tem cells displayed the highest cytotoxic score among T cell subsets, while CD8 + Tex cells showed a slight reduction in cytotoxicity compared to CD8 + Tem cells (Fig. 2C; Additional file 2: Fig. S2C). The proportions of CD8 + Tex and CD8 + Tprolif cells were significantly increased in immune-related myocarditis (Fig. 2D), indicating that CD8 + T cells continued to replicate and gradually became exhausted during chronic antigen exposure and sustained inflammatory stimulation.

Given that CD8 + Tem cells constituted a significant proportion of both the irAE and normal groups, we compared the signatures of CD8 + Tem cells between the two groups. Notably, CD8 + Tem cells exhibited significantly lower cytotoxicity in immune-related myocarditis than other samples in the normal group, whereas they showed increased exhaustion scores in the irAE group (Fig. 2E). This might be explained by the transition of CD8 + T cells from the effector memory state to the exhausted state in immune-related myocarditis. In addition, we investigated the metabolic characteristics of all T/NK subsets in irAE and normal heart tissues. Compared with those

in normal heart tissues, all subpopulations of lymphocytes in myocarditis tissue showed decreased oxidative phosphorylation and fatty acid oxidation pathway activities (Fig. 2F). This could be explained by a metabolic shift from oxidative phosphorylation to aerobic glycolysis under inflammatory conditions, enabling sufficient energy generation for cell proliferation and cytokine synthesis [44]. We evaluated the glycolysis pathway enrichment of all T/NK cells and found that lymphocytes in immune-related myocarditis significantly upregulated glycolysis metabolic activities (Fig. 2G), confirming the metabolic switch from oxidative phosphorylation to glycolysis. Moreover, the O-glycan and N-glycan biosynthesis pathways were found to be upregulated in lymphocytes in the irAE group (Fig. 2F). Previous studies reported that O-glycans might play a role in leukocyte trafficking to inflamed tissues [45, 46] and N-glycans might be related to ligand-receptor binding during immune responses [47], potentially exacerbating inflammation in immune-related myocarditis.

Enhanced pro-inflammatory signatures in myeloid cells in immune-related myocarditis

Myeloid cells were classified into 6 subpopulations based on cluster-specific markers (Fig. 3A, B; Additional file 2: Fig. S3A, B). To explore the relationships among the subsets of monocytes/macrophages, we performed trajectory analysis on antigen-presenting macrophages, LYVE1 + macrophages, CD14 + monocytes, and CD16 + monocytes. The trajectory started from CD14 + monocytes, transited through CD16 + monocytes, and bifurcated into two branches toward antigen-presenting macrophages and LYVE1 + macrophages (Fig. 3C; Additional file 2: Fig. S3C). DEGs along the trajectory were identified, and tissue-resident markers of LYVE1 + macrophages, including *COLEC12*, *F13A1*, *LYVE1*, *CD209*, and *FOLR2*, were upregulated at the later stage of pseudotime (Additional file 2: Fig. S3D) [48, 49]. LYVE1 + macrophages resided in the heart and played a crucial role in tissue homeostasis maintenance and anti-inflammation [41]. Antigen-presenting macrophages showed high expression levels of cytokine genes such as *CCL3L1*, *CCL3*, *CCL4*, *CXCL9*, and *CXCL10* as well as antigen-presentation genes such as *HLA-DQB1*, *HLA-DPA1*, *HLA-DQA1*, *HLA-DPB1*, and *HLA-DRB5*, indicating their essential role in immune cell recruitment and regulation of immune responses (Additional file 2: Fig. S3E). The proportion of antigen-presenting macrophages in the irAE group was higher than that in the normal group, which might explain the higher inflammatory levels in immune-related myocarditis (Fig. 3D).

Moreover, to study the transcriptomic differences of myeloid cells between immune-related myocarditis and normal heart tissues, we identified DEGs between the two groups. Notably, myeloid cells in the irAE group exhibited significant upregulation of genes related to cytokines or chemokines (*IL1B*, *CCL2*, *CCL3*, *CCL4*, *CCL3L1*, *CXCL2*, *CXCL3*, *CXCL8*, and *CXCL9*), major histocompatibility complex (MHC) proteins (*HLA-DRB5*, *HLA-DQA1*, *HLA-DQB1*, *HLA-DPA1*, and *HLA-B*), interferon signaling (*IFI30*), and tumor necrosis factor (*TNF*) (Fig. 3E; Additional file 1: Table S3). Functional enrichment analysis showed that upregulated genes in irAE were associated with cytokine production and leukocyte migration, activation, and differentiation, as well as inflammatory pathways such as the NF-κB, TNF, IL-17, and chemokine signaling pathways (Fig. 3F). GSEA revealed that myeloid cells in the irAE group were enriched in GO pathways such as adaptive immune response, cytokine-mediated signaling pathway, leukocyte migration, and positive regulation of leukocyte cell-cell adhesion (Additional file 2: Fig. S3F), as well as hallmark pathways including TNFα signaling via NF-κB, inflammatory response, and hypoxia (Fig. 3G, H). Notably, the oxidative phosphorylation pathway activity was significantly downregulated in myeloid cells in immune-related myocarditis (Fig. 3H). The inflammatory processes in myocarditis might induce a hypoxic microenvironment, thereby inhibiting electron transport in myeloid cells and suppressing oxidative phosphorylation [44]. We next evaluated the inflammatory signatures of monocyte/macrophage subsets in the irAE and normal groups. Among the four monocyte/macrophage subpopulations, antigen-presenting macrophages exhibited the highest M1 and pro-inflammatory scores, while LYVE1 + macrophages showed higher M2 scores than M1 scores, consistent with their role in homeostatic regulation as tissue-resident macrophages (Fig. 3I). Moreover, antigen-presenting macrophages, CD14 + monocytes, and CD16 + monocytes in the irAE group exhibited significantly higher M1 and pro-inflammatory scores than those in the normal group, consistent with previous findings suggesting that pro-inflammatory macrophages showed impaired oxidative phosphorylation metabolism and relied primarily on glycolysis instead [50, 51].

Enhanced intercellular communications among immune cells in immune-related myocarditis

The interplay among immune cells directly contributes to inflammation and leads to damage to myocardial tissue. Consequently, we compared intercellular communications among immune cells between the irAE group and the normal group. We observed heightened interaction strength among immune cells with increased enrichment of pathways including CCL, CXCL, MHC-II, and TNF in the irAE group, revealing a more pronounced inflammatory state in immune-related myocarditis (Fig. 4A; Additional file 2: Fig.

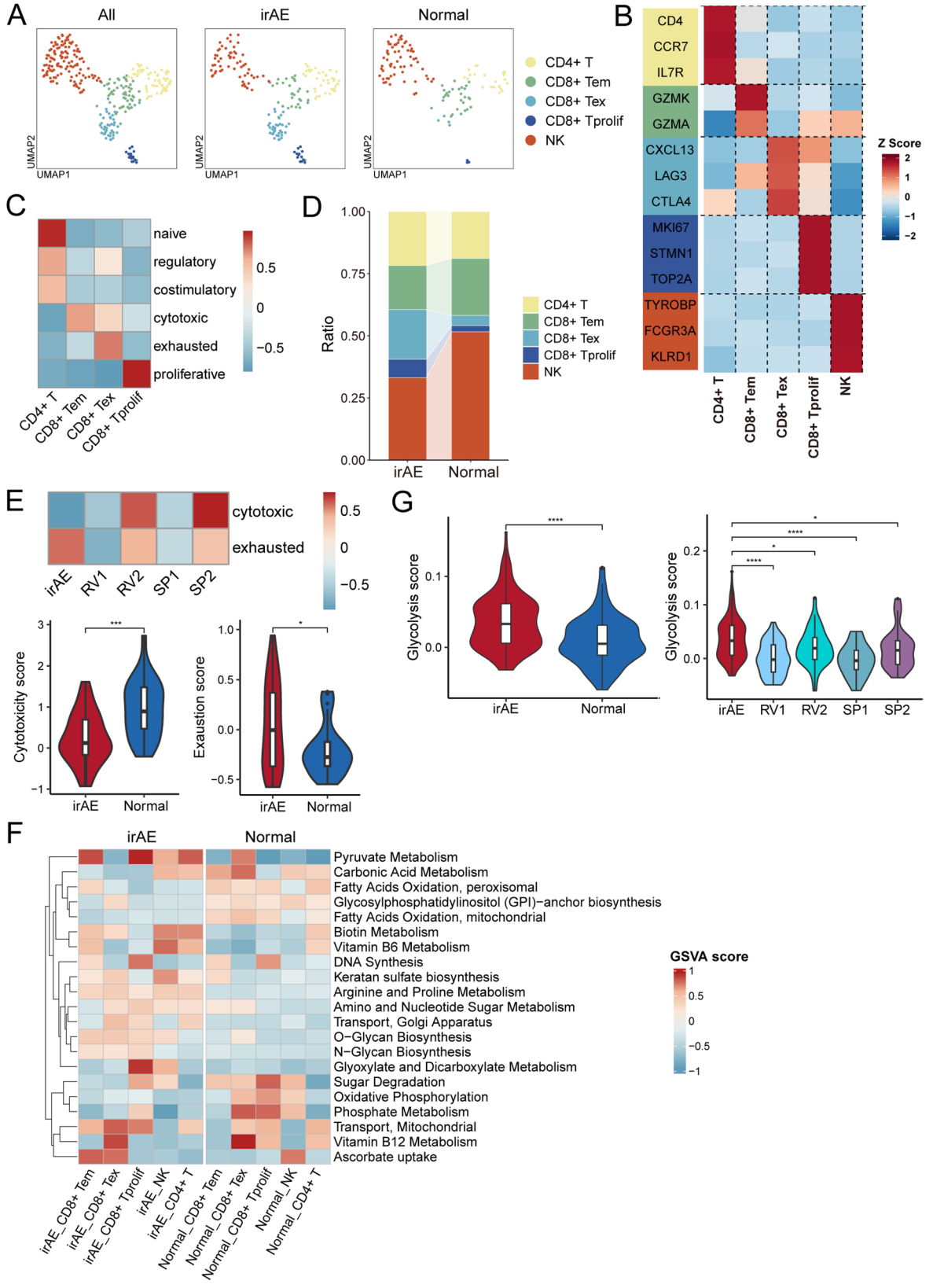

Fig. 2 (See legend on next page.)

(See figure on previous page.)

Fig. 2 CD8 + T cells were converted to exhausted states in the irAE group. (**A**) UMAP projection of all lymphocytes across all samples as well as the irAE and normal groups, respectively. (**B**) Heatmap of marker gene expression of T/NK subpopulations. (**C**) Heatmap showing the signature scores of T cell subpopulations, including naive, regulatory, costimulatory, cytotoxic, exhausted, and proliferative. (**D**) Proportions of T/NK subpopulations in the irAE and normal groups. (**E**) Cytotoxic and exhausted signature scores of CD8 + Tem cells in the irAE and normal groups. P values were determined by the Wilcoxon test. (**F**) Metabolic activity scores of T/NK subpopulations in the irAE and normal groups. (**G**) Violin plots showing the glycolysis scores of lymphocytes in the irAE and normal groups. P values were determined by the Wilcoxon test. * $p < 0.05$, ** $p < 0.01$, *** $p < 0.001$, and **** $p < 0.0001$ were considered statistically significant. CD8 + Tem, CD8 + effector memory T; CD8 + Tex, CD8 + exhausted T; CD8 + Tprolif, CD8 + proliferative T; NK, natural killer; UMAP, Uniform Manifold Approximation and Projection; irAE, immune-related adverse event

S4A). Stronger intercellular interactions were identified in the irAE group, with myeloid cells acting as senders and lymphocytes acting as receivers (Fig. 4B). Antigen-presenting macrophages, CD14 + monocytes, and CD16 + monocytes demonstrated stronger interactions with other immune cells in immune-related myocarditis (Fig. 4C). Further investigation of the CCL pathway revealed more signals sent from antigen-presenting macrophages, CD14 + monocytes, and CD16 + monocytes to CD8 + T cells and NK cells in the irAE group (Fig. 4D; Additional file 2: Fig. S4B). Antigen-presenting macrophages, CD14 + mono, and CD16 + mono were also key sources of signaling in the upregulated TNF pathway network of immune-related myocarditis, with S100P – neutrophils, S100P + neutrophils, and T/NK cells being the primary receivers (Fig. 4E; Additional file 2: Fig. S4C). The top ligand-receptor pairs between myeloid cells and lymphocytes significantly upregulated in the irAE group included TNF–TNFRSF1B, CCL4–CCR5, CCL3–CCR5, CCL3–CCR1, and CCL3L1–CCR1 (Fig. 4F). Furthermore, enhanced interactions of S100P – and S100P + neutrophils with CD8 + Tex cells through CXCL16–CXCR6 were also observed in the irAE group (Fig. 4F). These findings might explain the heightened secretion of inflammatory cytokines and the increased recruitment of immune cells to heart tissue in immune-related myocarditis, identifying potential therapeutic targets to inhibit immune cell interactions and alleviate myocarditis severity.

Augmented inflammatory responses related to endothelial cells in immune-related myocarditis

As non-immune cells constituted the vast majority of cells in heart tissue, we subsequently conducted a detailed investigation into subpopulations of vascular cells and fibroblasts. Within vascular cells, in addition to smooth muscle cells and pericytes, we identified 5 subsets of endothelial cells: arterial ECs (*HEY1* + *SEMA3G*+), capillary ECs (*RGCC* + *CA4*+), immune capillary ECs (*CX3CL1* + *GBP1*+), venous ECs (*ACKR1* + *PLVAP*+), and lymphatic ECs (*TBX1* + *PROX1*+) (Fig. 5A, B; Additional file 2: Fig. S5A, B). GO analysis was performed on the genes upregulated in venous ECs, and pathways associated with cytokine binding, MHC-II protein function, and leukocyte activation and adhesion were enriched (Fig. 5C). These results might suggest a crucial role for venous ECs in inflammatory regulation, consistent with the findings of a previous study [52]. Moreover, we identified DEGs of endothelial cells between the irAE group and the normal group and found that endothelial cells in immune-related myocarditis significantly upregulated genes related to inflammatory chemokines (*CCL2*, *CXCL3*, *CX3CL1*, and *CXCL12*), antigen presentation (*CD74*, *HLA-DPA1*, *HLA-DRB5*, and *HLA-B*), *TNF*, and inflammation-related transcription factors (*FOSB*, *JUN*, *JUNB*, and *JUND*) (Fig. 5D; Additional file 1: Table S4). These upregulated genes in the irAE group were enriched in pathways including antigen processing and presentation, the TNF signaling pathway, the IL17 signaling pathway, Th17 cell differentiation, and viral myocarditis (Fig. 5E). These findings indicated that endothelial cells in immune-related myocarditis displayed close connections with immune cells, potentially contributing to the dissemination and amplification of inflammation.

CXCL9 + fibroblasts were expanded in immune-related myocarditis

We next explored the heterogeneity of fibroblasts and identified 4 subsets based on the expression of cluster-specific marker genes: GPX3 + Fibro, BTG2 + Fibro, CXCL9 + Fibro, and POSTN + Fibro (Fig. 6A, B; Additional file 2: Fig. S6A, B). GPX3 + and POSTN + fibroblasts were present in both immune-related myocarditis and normal cardiac tissues, whereas CXCL9 + and BTG2 + fibroblasts were almost exclusively found in tissues with myocarditis (Fig. 6A). GO analysis showed the enrichment of GPX3 + fibroblasts and POSTN + fibroblasts in pathways related to extracellular matrix organization, essential for cardiac tissue homeostasis (Fig. 6C). BTG2 + fibroblasts were enriched in stress response pathways such as response to unfolded protein, response to topologically incorrect protein, and unfolded protein binding, suggesting the stressed conditions in immune-related myocarditis (Fig. 6C). CXCL9 + fibroblasts exhibited high expression levels of chemokine genes (*CXCL9* and *CXCL10*) and antigen-presenting genes (*CD74* and HLA class II genes) and were enriched in pathways involved in antigen processing and presentation, MHC protein complex assembly, and response to type II interferon (Fig. 6B, C; Additional file 2: Fig. S6C).

As CXCL9 + fibroblasts were rarely present in healthy heart tissues, we extensively investigated the function of

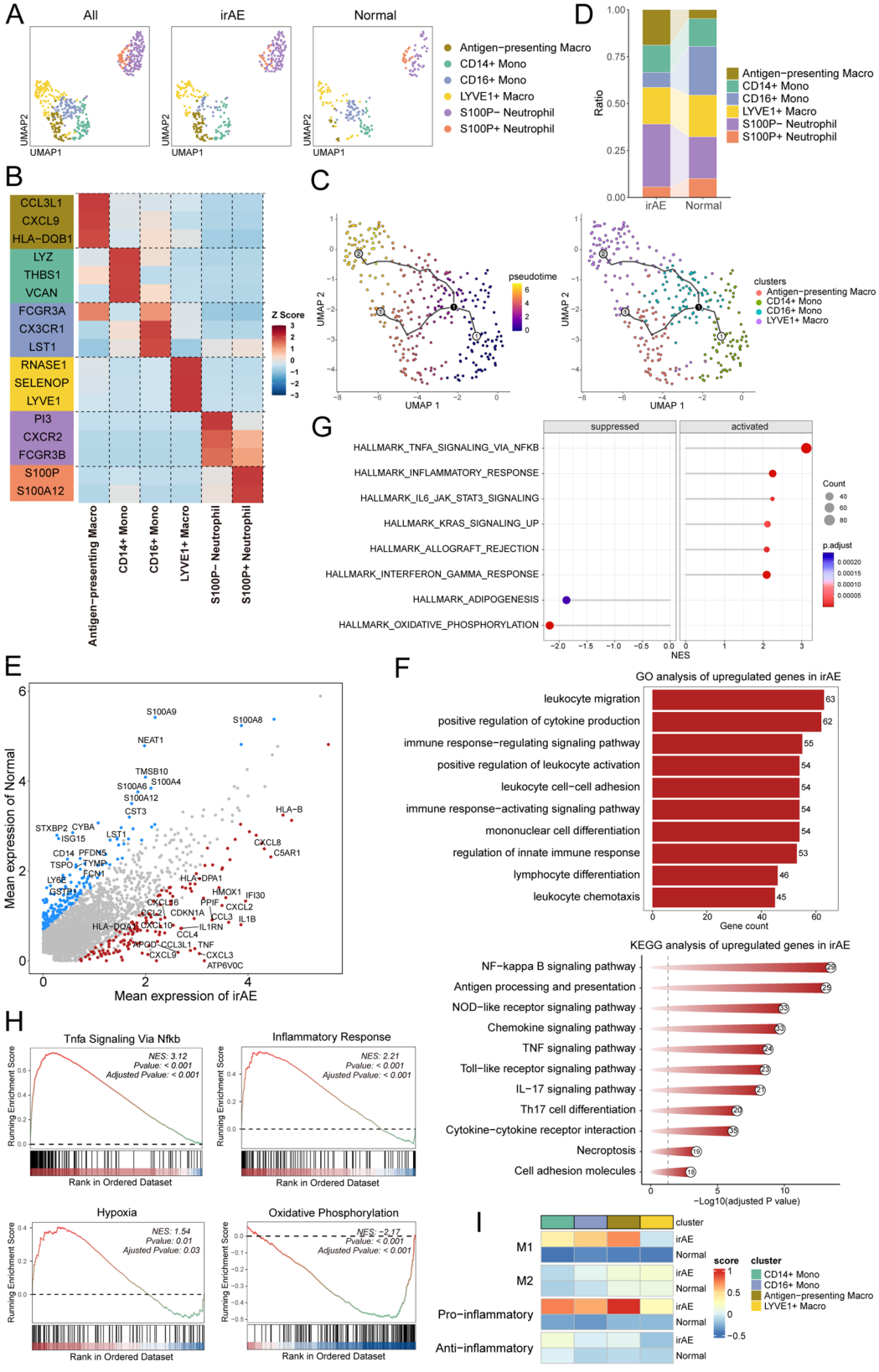

Fig. 3 (See legend on next page.)

(See figure on previous page.)

Fig. 3 Upregulation of pro-inflammation signatures in myeloid cells in the irAE group. (**A**) UMAP projection of all myeloid cells across all samples as well as the irAE and normal groups, respectively. (**B**) Heatmap of marker gene expression of myeloid cell subpopulations. (**C**) Monocle3 pseudotime trajectory showing the developmental paths of monocyte/macrophage subsets. (**D**) Proportions of myeloid cell subpopulations in the irAE and normal groups. (**E**) Volcano plot showing DEGs of myeloid cells between the irAE group and the normal group. (**F**) Top enriched Gene Ontology (GO) and Kyoto Encyclopedia of Genes and Genomes (KEGG) pathways of DEGs upregulated in myeloid cells in the irAE group. (**G**) Gene set enrichment analysis (GSEA) showing activated and suppressed hallmark pathways of myeloid cells in the irAE group. (**H**) GSEA revealing upregulation of pathways including TNFα signaling via NFκB, inflammatory response, and hypoxia, as well as downregulation of oxidative phosphorylation pathway in myeloid cells in the irAE group. (**I**) Heatmap showing the M1, M2, pro-inflammatory, and anti-inflammatory signature scores of monocyte/macrophage subsets in the irAE and normal groups. LYVE1, lymphatic vessel endothelial hyaluronan receptor 1; S100P, S100 calcium binding protein P; Antigen-presenting Macro, antigen-presenting macrophage; CD14 + Mono, CD14 + monocyte; CD16 + Mono, CD16 + monocyte; LYVE1 + Macro, LYVE1 + macrophage; NES, normalized enrichment score; UMAP, Uniform Manifold Approximation and Projection; irAE, immune-related adverse event

CXCL9 + fibroblasts in immune-related myocarditis. We first calculated the pathway activities of four fibroblast subclusters and found that CXCL9 + fibroblasts showed high activities in the JAK-STAT and TNFα pathways, which were closely associated with inflammatory and autoimmune diseases (Fig. 6D) [53, 54]. Additionally, we inferred the transcription factors regulating each fibroblast subset and found that the activities of many transcription factors were upregulated in CXCL9 + fibroblasts (Additional file 2: Fig. S6D). Compared to those in the other three clusters, transcription factors enriched in CXCL9 + fibroblasts were related to MHC class II gene expression (*CIITA*, *RFXAP*, *RFXANK*, and *RFX5*) [55, 56] and interferon signaling pathways (*IRF1*, *IRF9*, and *STAT1*) [57], contributing to the heightened immune response in immune-related myocarditis (Fig. 6E). To further investigate the cytokine signaling profiles of CXCL9 + fibroblasts, we applied Cytosig to predict the cytokine signatures of the four fibroblast subclusters. Consistent with the findings of the pathway analysis and transcription factor analysis, CXCL9 + fibroblasts demonstrated elevated activities of pro-inflammatory cytokine pathways such as IFNG, PDGFD, IL1B, and TNFA, and downregulated expression of anti-inflammatory cytokine signaling pathways IL4 and IL10 (Fig. 6F) [58]. These findings revealed the crucial role of CXCL9 + fibroblasts in presenting antigens to immune cells, producing and responding to cytokines, and thereby promoting inflammation.

The interaction between stromal cells and immune cells contributed to inflammation in immune-related myocarditis

As endothelial cells and fibroblasts participated significantly in inflammation, we explored the cell-cell communications between stromal cells and immune cells in heart tissue. Interestingly, in the CXCL and CCL signaling pathway networks, venous ECs were the main signaling receiver and antigen-presenting macrophages were the major sender (Fig. 7A, B). CD14 + monocytes and CXCL9 + fibroblasts also contributed to the CXCL pathway by producing CXC-chemokines (Fig. 7A). As myeloid cells were the main providers of CXCL signaling, we next compared the differences in the CXCL pathway between myeloid cells and venous ECs in the irAE group and the normal group. In immune-related myocarditis, the CXCL pathways exhibited increased enrichment between venous ECs and myeloid cells including antigen-presenting macrophages, CD14 + monocytes, and CD16 + monocytes, as compared to normal heart tissues (Fig. 7C). The ligand-receptor pair analysis revealed that CXCL2–ACKR1, CXCL3–ACKR1, CXCL8–ACKR1, and CXCL9–ACKR1 interactions were enriched in immune-related myocarditis (Fig. 7D). Atypical chemokine receptor-1 (*ACKR1*) was highly expressed in venous ECs (Fig. 5B) and was involved in the transcytosis of chemokines from the subluminal to luminal side upon binding to them, thereby facilitating the recruitment of circulating leukocytes to the inflamed tissues [59].

Furthermore, CXCL9 + fibroblasts were also identified as an important source of CXCL and CCL signaling pathways (Fig. 7A, B), prompting us to further investigate their interactions with other cells. Notably, among the four fibroblast subsets, CXCL9 + fibroblasts demonstrated the most significant enrichment of signaling pathways toward lymphocytes and myeloid cells, such as the MHC-I, MHC-II, CXCL, and CCL pathways. It indicated that CXCL9 + fibroblasts showed strong interactions with immune cells, primarily through the presentation of antigens or the production of chemokines by lymphocytes and myeloid cells (Additional file 2: Fig. S7A, B). Additionally, we explored the interactions between fibroblasts and endothelial cells and found a notable enrichment of CXCL pathways between CXCL9 + fibroblasts and venous ECs (Fig. 7E; Additional file 2: Fig. S7C). Among the CXCL and CCL pathways, the most significantly enriched ligand-receptor pairs between CXCL9 + fibroblasts and venous ECs included CXCL2–ACKR1, CXCL8–ACKR1, CXCL9–ACKR1, CXCL10–ACKR1, and CXCL11–ACKR1, with CCL2–ACKR1 exhibiting notable prominence (Fig. 7F). CXCL9 + fibroblasts exhibited robust interactions with venous ECs and the chemokines produced by CXCL9 + fibroblasts could undergo transcytosis by venous ECs and enter the bloodstream, thereby enhancing leukocyte recruitment and exacerbating cardiac tissue inflammation.

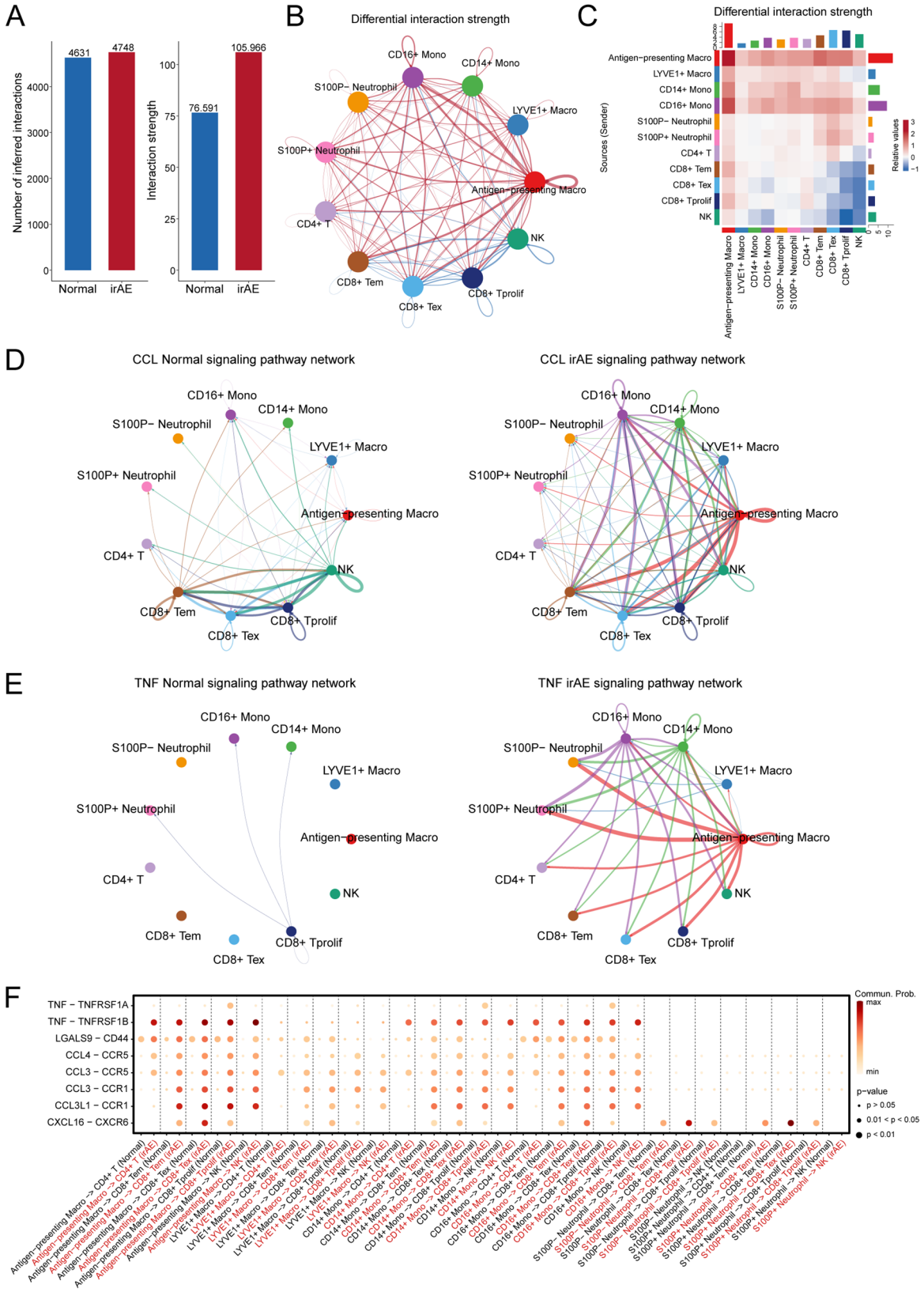

Fig. 4 (See legend on next page.)

(See figure on previous page.)

Fig. 4 Increased cell-cell communications among immune cells in the irAE group. (**A**) Bar plots showing the number of interactions and interaction strength among immune cells in the irAE and normal groups. (**B**) Circle plot showing differential interaction strength among immune cell subpopulations between the irAE group and the normal group. Red colored lines represent increased signaling and blue colored lines represent decreased signaling in the irAE group. (**C**) Heatmap illustrating differential interaction strength among immune cell subsets in the irAE group vs. the normal group. The x-axis represents the signaling receivers and the y-axis represents the signaling senders. (**D**) Circle plots showing the CCL signaling pathway networks among immune cells in the irAE and normal groups. (**E**) Circle plots showing the TNF signaling pathway networks among immune cells in the irAE and normal groups. (**F**) Bubble plot showing the enriched ligand-receptor pairs among immune cells with color representing the communication probability and size reflecting the p-value significance. CD8 + Tem, CD8 + effector memory T; CD8 + Tex, CD8 + exhausted T; CD8 + Tprolif, CD8 + proliferative T; NK, natural killer; Antigen-presenting Macro, antigen-presenting macrophage; CD14 + Mono, CD14 + monocyte; CD16 + Mono, CD16 + monocyte; LYVE1 + Macro, LYVE1 + macrophage; CCL, C-C motif chemokine ligand; TNF, tumor necrosis factor; irAE, immune-related adverse event

Murine single-cell profiling validated unique immune and stromal characteristics in immune-related myocarditis

To validate the inflammatory features of human immune-related myocarditis and assess their specificity to ICI-related pathology, we analyzed mouse scRNA-seq data, comparing ICI-related myocarditis with controls, as well as with viral and autoimmune myocarditis. The major cell subpopulations were also identified in mice (Fig. 8A; Additional file 2: Fig. S8A-D). As only CD45 + cells were available for autoimmune myocarditis, it was excluded from stromal cell comparisons.

Across the four conditions, the irAE group showed the highest proportion of T/NK cells among all immune cells (Additional file 2: Fig. S8E). Consistent with human data, exhausted CD8 + T cells were significantly enriched in immune-related myocarditis compared to controls, as well as viral and autoimmune myocarditis (Fig. 8B; Additional file 2: Fig. S9A-C). T/NK cells in the irAE group exhibited the highest overall expression of exhaustion signatures (Fig. 8C), suggesting lymphocyte exhaustion as a distinct feature of immune-related myocarditis. Additionally, T/NK cells in the irAE group had higher glycolysis scores than controls but lower than the autoimmune group (Fig. 8C). Within the myeloid compartment, we identified a cluster resembling antigen-presenting macrophages in human hearts, showing high *Cxcl9* and antigen-presentation genes (*H2-DMb1*, *H2-DMb2*, and *H2-DMa*) expression, which was designated as Macro_Cxcl9 (Additional file 2: Fig. S10A-C). Another subset, Macro_Folr2, highly expressed tissue-resident markers *Folr2* and *Lyve1*, recapitulating the phenotype of human LYVE1 + macrophages (Additional file 2: Fig. S10A-C). Across conditions, monocyte/macrophage subsets in the irAE group exhibited the highest M1 and pro-inflammatory signatures, with Macro_Cxcl9 being the most prominent (Fig. 8D). DEGs upregulated in the irAE group compared to the other groups were consistently enriched in immune activation and immune response regulation pathways, underscoring the unique characteristics of myeloid cells in immune-related myocarditis (Additional file 2: Fig. S10D-F).

Murine endothelial cell subpopulations largely corresponded to their human counterparts (Additional file 2: Fig. S11A-C), though venous ECs lacked expression of *Ackr1*, a marker gene for human venous ECs (Additional file 2: Fig. S11D). Compared to controls, endothelial cells in the irAE group exhibited upregulated genes enriched in multiple inflammatory pathways, whereas those upregulated relative to the viral group were linked to metabolism and immune cell chemotaxis (Additional file 2: Fig. S11E, F). The Tnf–Tnfrsf1a interaction between macrophages and ECs was stronger in the irAE group than in the control group (Fig. 8E). Ccl chemokine–Ackr2 interactions were enriched exclusively between macrophages and lymphatic ECs in the irAE group, reflecting a species-specific mechanism of leukocyte recruitment (Fig. 8E). We also identified a fibroblast cluster, Fibro_Cxcl10, characterized by high expression of *Cxcl9*, *Cxcl10*, interferon-stimulated genes (*Gbp4*, *Gbp6*, *Gbp10*, and *Stat1*), and MHC-I genes (*H2-Q4*, *H2-Q6*, and *H2-Q7*) (Additional file 2: Fig. S12A-C). This cluster was significantly enriched in the irAE group, with higher levels than in the control and viral myocarditis samples (Fig. 8F). It exhibited strong activation of the JAK-STAT and TNFα pathways and was highly involved in immune response regulation (Fig. 8G; Additional file 2: Fig. S12D). Intercellular communication analysis identified Cxcl10 + fibroblasts as the most prominent signaling senders (Fig. 8H), highly paralleling the role of human CXCL9 + fibroblasts (Fig. 6G). They maintained extensive interactions with other stromal and immune cells (Additional file 2: Fig. S12E), underscoring their involvement in myocarditis progression.

Discussion

Immune-related myocarditis is rare but can be life-threatening. Elucidating the mechanisms underlying immune-related myocarditis is crucial for identifying key pro-inflammatory cells, identifying potential therapeutic targets, and improving patient prognosis. Current single-cell research primarily utilizes mouse models and focuses on immune cells, and further investigations into the role of stromal cells within the myocarditis microenvironment in humans are lacking. In this study, we performed scRNA-seq on the endomyocardial biopsy sample obtained from a patient with immune-related myocarditis and used heart specimens from donors without heart diseases as the control group. We conducted a

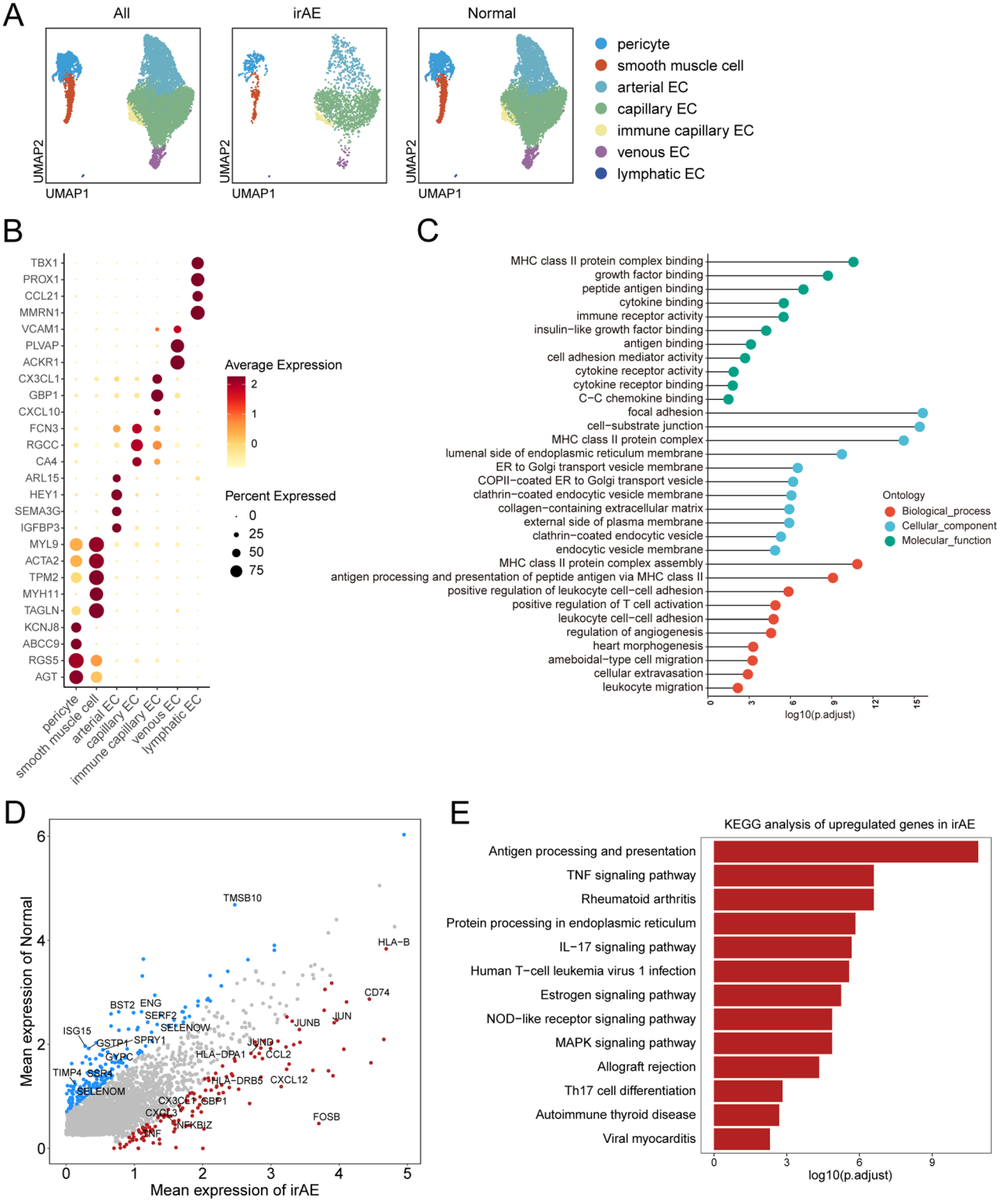

Fig. 5 Endothelial cells were closely associated with immune-related myocarditis. (**A**) UMAP projection of all vascular cells across all samples as well as the irAE and normal groups, respectively. (**B**) Dot plot showing the expression levels of marker genes of each subpopulation. (**C**) GO analysis of specific marker genes of venous ECs. (**D**) Volcano plot showing DEGs of endothelial cells between the irAE group and the normal group. (**E**) Top enriched KEGG pathways of upregulated genes of endothelial cells in the irAE group. arterial EC, arterial endothelial cell; capillary EC, capillary endothelial cell; immune capillary EC, immune capillary endothelial cell; venous EC, venous endothelial cell; lymphatic EC, lymphatic endothelial cell; UMAP, Uniform Manifold Approximation and Projection; irAE, immune-related adverse event

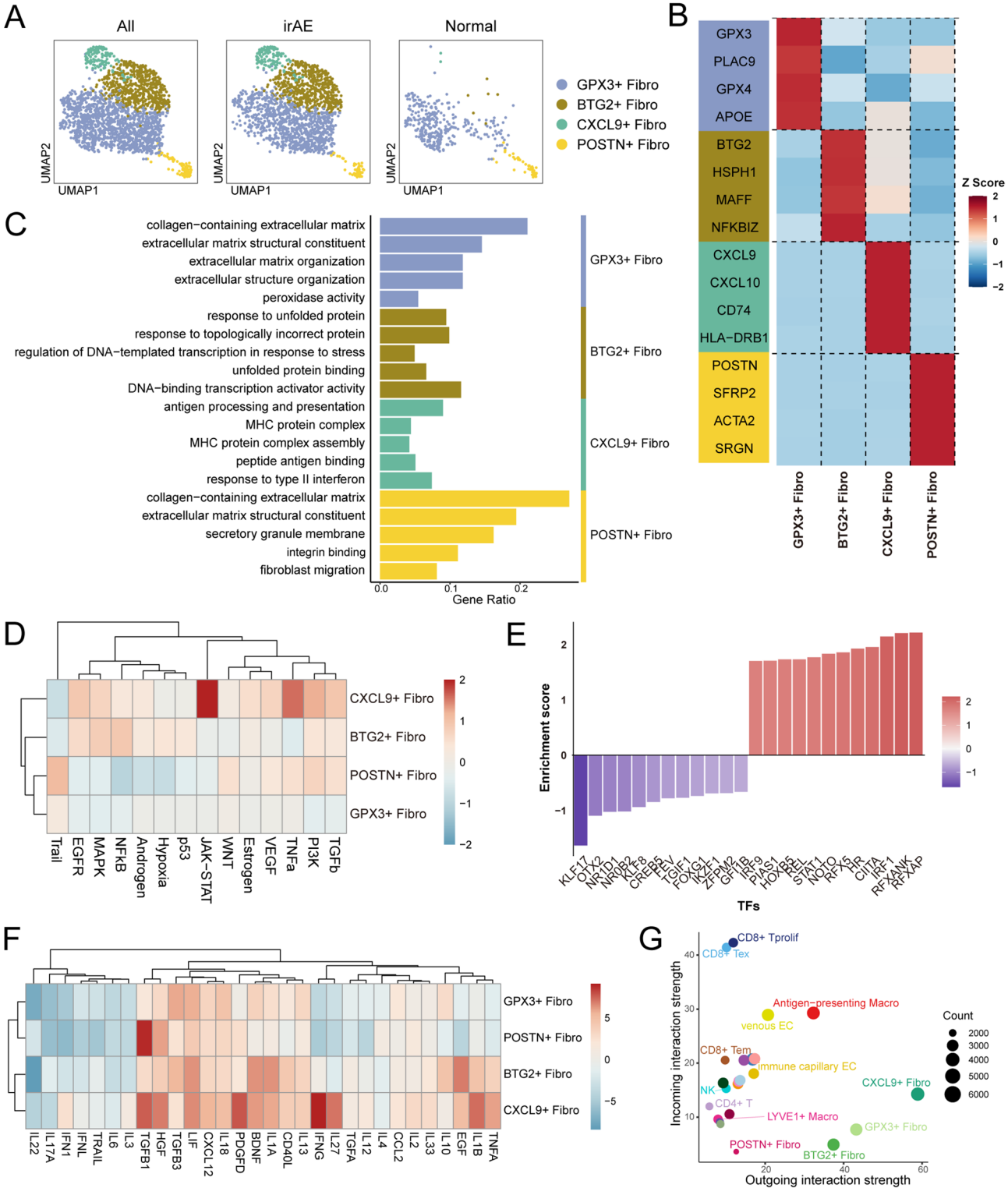

Fig. 6 CXCL9 + fibroblasts played an important role in inflammation. (**A**) UMAP projection of all fibroblasts across all samples as well as the irAE and normal groups, respectively. (**B**) Heatmap showing marker gene expression of fibroblast subpopulations. (**C**) Enriched GO pathway terms of marker genes of each fibroblast subpopulation. (**D**) Heatmap of normalized PROGENy pathway activity scores of fibroblast subpopulations. (**E**) Bar plot showing the enrichment scores of top transcription factors upregulated (red) and downregulated (blue) in CXCL9 + fibroblasts. (**F**) Heatmap showing the cytokine signaling scores of four fibroblast subsets. (**G**) Incoming and outgoing interaction strengths of all cell clusters in human heart tissues. GPX3 + Fibro, GPX3 + fibroblast; BTG2 + Fibro, BTG2 + fibroblast; CXCL9 + Fibro, CXCL9 + fibroblast; POSTN + Fibro, POSTN + fibroblast; TFs, transcription factors; UMAP, Uniform Manifold Approximation and Projection; irAE, immune-related adverse event

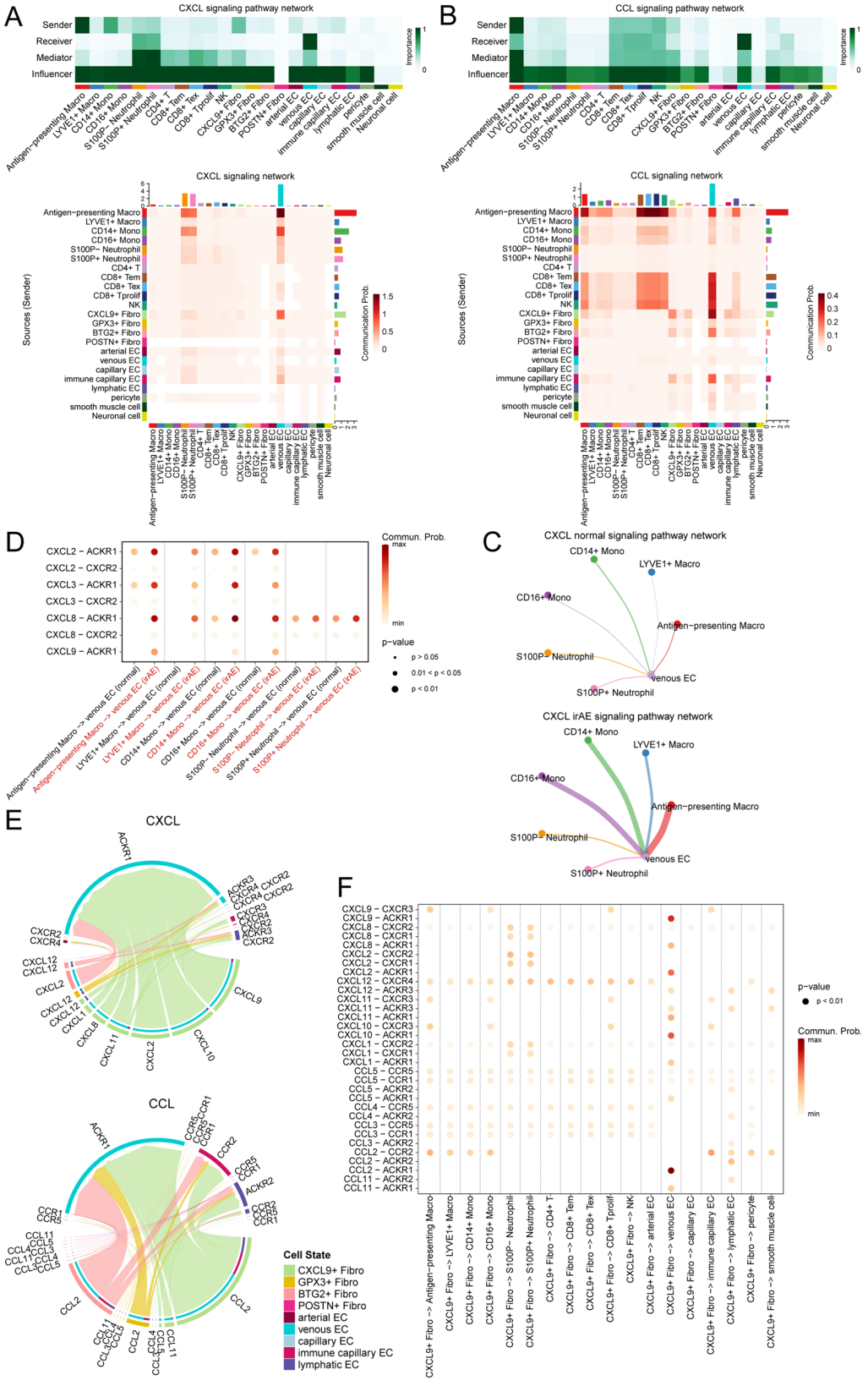

Fig. 7 (See legend on next page.)

(See figure on previous page.)

Fig. 7 The interaction between stromal cells and immune cells contributed to inflammation in immune-related myocarditis. (**A**) Heatmaps showing the signaling roles and contributions of cell subpopulations in the CXCL signaling pathway network. (**B**) Heatmaps showing the signaling roles and contributions of cell subpopulations in the CCL signaling pathway network. (**C**) Interaction strengths of CXCL signaling pathways between myeloid cell subpopulations (senders) and venous ECs (receivers) in the irAE and normal groups. (**D**) Bubble plot showing the enriched ligand-receptor pairs of CXCL signaling pathways between myeloid cell subpopulations and venous ECs in the irAE and normal groups. (**E**) Chord diagrams of CCL and CXCL signaling pathways between fibroblast subpopulations (senders) and endothelial cell subpopulations (receivers). (**F**) Bubble plot showing the enriched ligand-receptor pairs of CCL and CXCL signaling pathways between CXCL9 + fibroblasts and other cells. CCL, C-C motif chemokine ligand; CXCL, C-X-C motif chemokine ligand; irAE, immune-related adverse event

detailed investigation into the functions of immune cells and stromal cells and compared their differences between the irAE and normal groups. Our analysis revealed an increase in immune cells and fibroblasts in immune-related myocarditis, contributing to cardiac inflammation, as well as the injury and repair of cardiomyocytes.

To elucidate the mechanisms of localized inflammation in immune-related myocarditis, we undertook a deeper investigation into the cellular subpopulations. Within the lymphocyte compartment, there was a greater proportion of CD8 + Tex and CD8 + Tprolif cells than in normal heart tissues, indicating that a highly inflammatory environment contributed to the exhaustion and proliferation of CD8 + T cells. Similar patterns have been reported in anti-PD-1-induced type 1 diabetes and immune-related colitis, where CD8 + T cells demonstrated a shift toward the terminally exhausted/effector-like phenotype, as compared to both non-irAE inflammatory tissues and healthy controls [60]. During pro-inflammatory responses, the activities of fatty acid oxidation and oxidative phosphorylation in immune cells are inhibited, whereas glycolysis is enhanced [61]. Consistently, in our study, the single-cell metabolic analysis of lymphocytes also revealed a shift from oxidative phosphorylation and fatty acid oxidation to glycolysis in immune-related myocarditis, revealing the highly inflammatory nature of this condition.

Antigen-presenting macrophages with high expression levels of cytokine and antigen-presentation genes, indicative of an inflammatory macrophage subpopulation, comprised a higher proportion in immune-related myocarditis. Myeloid cells in immune-related myocarditis significantly upregulated genes related to antigen presentation, immune cell migration, and inflammatory pathways. Moreover, myeloid cells in the irAE group also exhibited upregulation of pathways associated with the inflammatory response and hypoxia, while demonstrating decreased activity of oxidative phosphorylation. The hypoxic environment in immune-related myocarditis induced by inflammatory interactions might prompt a metabolic switch from oxidative phosphorylation to glycolysis, thereby increasing the expression of M1 and pro-inflammatory patterns [44]. Within the microenvironment of immune-related myocarditis, antigen-presenting macrophages were the primary signaling sender of multiple inflammatory pathways, including CXCL, CCL, and TNF. Compared to normal heart tissues, antigen-presenting macrophages in the irAE group showed significantly enhanced interactions with T/NK cells, with enriched ligand-receptor pairs such as TNF–TNFRSF1B, CCL3–CCR1, and CCL3L1–CCR1. The CCL/CXCL pathways increase the recruitment of T/NK cells and the TNF–TNFRSF1B signaling pathway can induce the activation of T/NK cells [62, 63]. The heightened intercellular interactions between myeloid cells and T/NK cells increased the quantity and activity of immune cells infiltrating the heart tissue, indicating a markedly more inflammatory microenvironment of immune-related myocarditis. Targeting these enriched ligand-receptor interactions could serve as a promising therapeutic approach for attenuating immune-related myocarditis.

As stromal cells constitute a substantial proportion of heart tissues, it is also essential to explore their contributions to immune-related myocarditis. Within the compartment of endothelial cells, venous ECs specifically expressed *ACKR1*, which encodes an atypical receptor for CXC- and CC-chemokines. ACKR1 enables the transcytosis of chemokines to the luminal surfaces of endothelial cells, thereby recruiting the circulating leukocytes [59]. Moreover, the expression of ACKR1 receptors on endothelial cell surfaces can promote the transendothelial migration of lymphocytes and myeloid cells through the chemotactic action of CXC- and CC-chemokines [64]. The interactions between endothelial cells and immune cells through ACKR1 and CXC-chemokines have also been observed in other autoimmune or inflammatory diseases, such as Hashimoto's thyroiditis [64], multiple sclerosis [65], interstitial cystitis [66], and inflammatory skin diseases [67], which highlights the significance of ACKR1 expression in inflammation. In our study, antigen-presenting macrophages, CD14 + monocytes, and CXCL9 + fibroblasts were identified as the primary sources of CXC-chemokines, while antigen-presenting macrophages were found to be the main producers of CC-chemokines. Inhibiting the interactions between these chemokines and ACKR1 might decrease immune cell recruitment to inflamed tissues, offering a potential therapeutic approach for immune-related myocarditis.

CXCL9 + fibroblasts were predominantly present in heart tissues affected by immune-related myocarditis. Consistently, a previous study also reported an expansion of CXCL10 + CCL19 + inflammatory fibroblasts

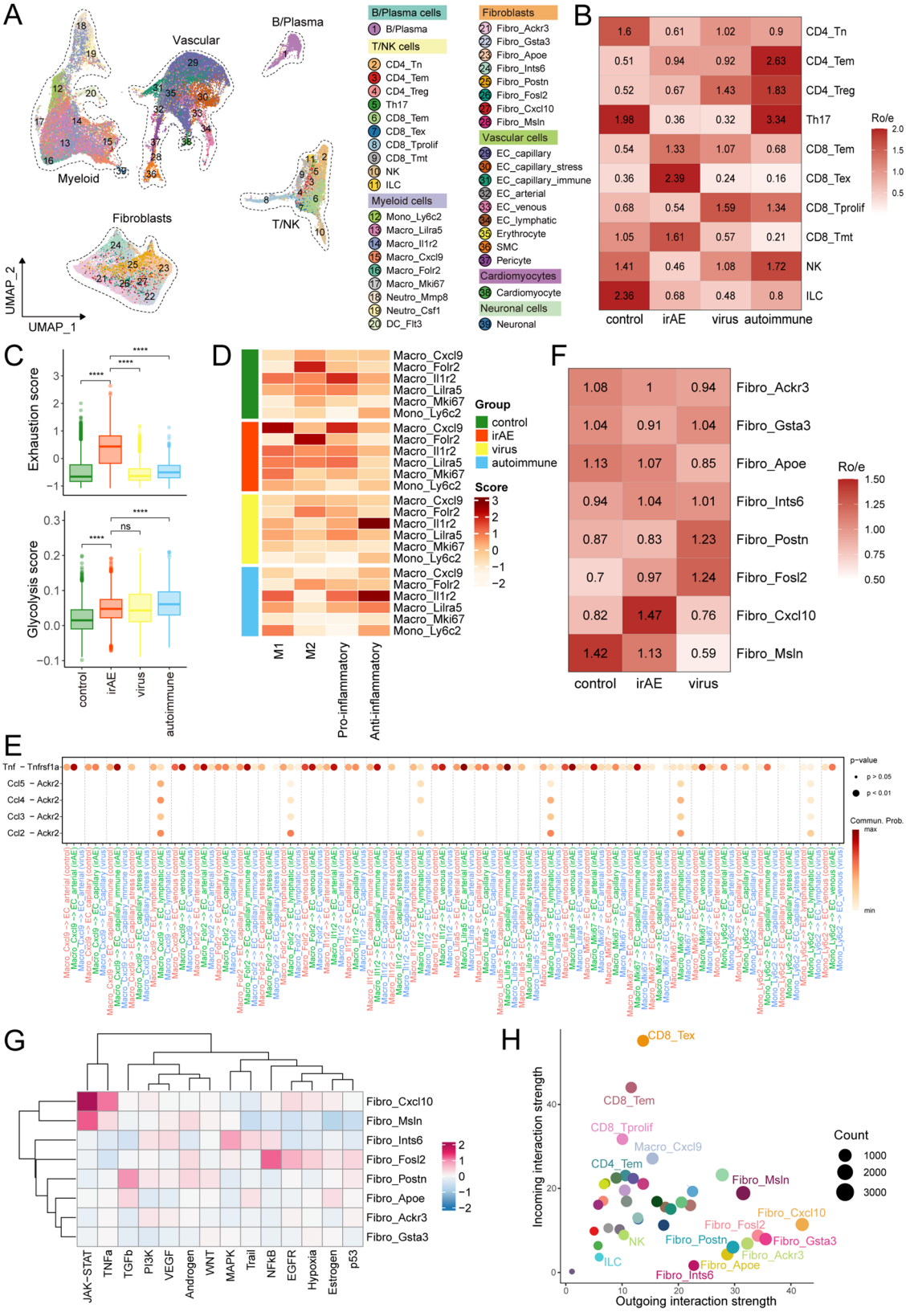

Fig. 8 (See legend on next page.)

(See figure on previous page.)

Fig. 8 Mouse single-cell transcriptomic analysis revealed distinct immune and stromal features of immune-related myocarditis. (**A**) UMAP projection of cardiac cell populations in murine hearts across four groups: control, irAE, viral, and autoimmune myocarditis. (**B**) Group prevalence of each T/NK cell subset estimated by the Ro/e score, representing the ratio of observed to expected cell numbers. (**C**) Boxplots showing the exhaustion and glycolysis signature scores of all T/NK cells in each group. P values were determined by the Wilcoxon test. (**D**) Heatmap showing the M1, M2, pro-inflammatory, and anti-inflammatory signature scores of monocyte/macrophage subpopulations across four groups. (**E**) Bubble plot showing the enriched ligand-receptor pairs of TNF and CCL signaling pathways between monocytes/macrophages and endothelial cells. (**F**) Group prevalence of each fibroblast subset estimated by the Ro/e score. (**G**) Heatmap of normalized PROGENy pathway activity scores of fibroblast subpopulations in murine hearts. (**H**) Incoming and outgoing interaction strengths of all cell subpopulations in murine heart tissues. * $p < 0.05$, ** $p < 0.01$, *** $p < 0.001$, and **** $p < 0.0001$ were considered statistically significant. irAE, immune-related adverse event; UMAP, Uniform Manifold Approximation and Projection; TNF, tumor necrosis factor; CCL, C-C motif chemokine ligand

in inflamed tissues compared to healthy tissues, across various diseases including rheumatoid arthritis, inflammatory bowel disease, interstitial lung disease, and Sjögren's syndrome [68]. We explored the inflammatory characteristics of CXCL9 + fibroblasts and found that CXCL9 + fibroblasts showed enrichment in JAK-STAT and TNFα pathways and upregulated transcription factors related to MHC class II gene expression and interferon signaling pathways. Additionally, CXCL9 + fibroblasts exhibited high expression of various pro-inflammatory cytokines, including IFNG, PDGFD, IL1B, and TNFA. Moreover, CXCL9 + fibroblasts exhibited close interactions with venous ECs through CXCL2–ACKR1, CXCL8–ACKR1, CXCL9–ACKR1, CXCL10–ACKR1, CXCL11–ACKR1, and CCL2–ACKR1, facilitating the transcytosis of chemokines produced by CXCL9 + fibroblasts and the recruitment of circulating immune cells. These findings indicate the significant pro-inflammatory role of CXCL9 + fibroblasts in immune-related myocarditis, highlighting its potential as a therapeutic target.

Our analysis of murine scRNA-seq data validated the key findings in humans and further delineated the distinct inflammatory microenvironment of immune-related myocarditis compared to other myocarditis types. The strong concordance between mouse and human cardiac cell populations supported the utility of mouse models in studying myocarditis pathogenesis. In murine ICI-related myocarditis, lymphocytes exhibited higher levels of exhaustion signatures compared to controls and remained higher than those in other myocarditis types. Myeloid cell subsets exhibited the highest M1-like and pro-inflammatory signatures, further highlighting the distinct immunopathological features of this condition. Moreover, Cxcl9 + Cxcl10 + fibroblasts identified in murine hearts shared key biological characteristics with human CXCL9 + fibroblasts, with heightened activity in the JAK-STAT and TNFα pathways and the strongest outgoing signaling toward other cell types. This subset was most abundantly enriched in mouse ICI-related myocarditis, indicating its role as a key pathogenic population uniquely associated with immune-related myocarditis. Unlike in humans, *ACKR1* expression was lacking in murine cardiac endothelial cells, in agreement with the review by Miranda et al. [41]. Nevertheless, endothelial cells in murine ICI-related myocarditis were still overall enriched for pathways associated with immune response regulation and immune cell chemotaxis, suggesting conserved features of immune-related myocarditis across species.

Several limitations of this study should be acknowledged. First, due to the invasive nature and limited diagnostic sensitivity, endomyocardial biopsy is rarely performed in clinical practice, which poses challenges in obtaining sufficient samples [69, 70]. Second, our analysis primarily focused on immune and stromal cells, while cardiomyocytes were not effectively captured owing to the technical constraints of droplet-based scRNA-seq platforms. Third, this study was limited to single-cell transcriptomic analysis and lacked integration with other omics approaches, such as spatial transcriptomics, proteomics, or epigenomics [71]. Future studies involving larger patient cohorts and multi-omics profiling are warranted to further explore microenvironmental differences among myocarditis subtypes and to identify potential therapeutic targets.

In summary, our single-cell analysis of immune-related myocarditis reveals distinct immune and stromal populations driving cardiac inflammation, offering insights into potential therapeutic strategies for this life-threatening irAE.

Abbreviations

ICIs	Immune checkpoint inhibitors
irAE	Immune-related adverse event
scRNA-seq	Single-cell RNA sequencing
ACKR1	Atypical chemokine receptor-1
PD-1	Programmed cell death 1
PD-L1	Programmed cell death 1 ligand 1
CTLA-4	Cytotoxic T lymphocyte-associated protein 4
TPS	Tumor proportion score
IFN	Interferon
NK	Natural killer
PBS	Phosphate-buffered saline
PCA	Principal component analysis
DEGs	Differentially expressed genes
GO	Gene Ontology
KEGG	Kyoto Encyclopedia of Genes and Genomes
GSEA	Gene set enrichment analysis
GSVA	Gene set variation analysis
CCA	Canonical correlation analysis
MHC	Major histocompatibility complex
TNF	Tumor necrosis factor

EC Endothelial cell

Supplementary Information

The online version contains supplementary material available at https://doi.org/10.1186/s12967-025-06551-x.

Supplementary Material 1

Supplementary Material 2

Acknowledgements
We thank Professor Yingxian Liu from the Department of Cardiology, Peking Union Medical College Hospital for assistance in collecting samples.

Author contributions
Conception and design: HTZ and HPW. Analysis and interpretation of data: BYS, ZYX, and ZXZ. Sample acquisition: LHZ and XQC. Manuscript writing: All authors. Revision of the manuscript: NZ, MJP, CJL, JYL, and SFL.

Funding
This work was supported by National High Level Hospital Clinical Research Funding (2022-PUMCH-C-054), Beijing Natural Science Foundation (L248022), National High Level Hospital Clinical Research Funding (2022-PUMCH-B-128), CAMS Innovation Fund for Medical Sciences (CIFMS) (2021-I2M-1-061, 2021-I2M-1-003), CSCO-hengrui Cancer Research Fund (Y-HR2019-0239, Y-HR2020MS-0415, Y-HR2020QN-0414), CSCO-MSD Cancer Research Fund (Y-MSDZD2021-0213) and National Ten-thousand Talent Program.

Data availability
The scRNA-seq data of the patient with immune-related myocarditis in this study are available upon reasonable request.

Declarations

Ethics approval and consent to participate
Ethical approval was obtained from the Ethics Committee of Peking Union Medical College Hospital (No. I-23PJ966). Written informed consent was provided by the patient.

Consent for publication
Not applicable.

Competing interests
The authors declare that they have no competing interests.

Author details
[1]Department of Pulmonary and Critical Care Medicine, State Key Laboratory of Complex Severe and Rare Diseases, Peking Union Medical College Hospital, Chinese Academy of Medical Sciences and Peking Union Medical College, No. 1 Shuaifuyuan, Beijing 100730, China
[2]Department of Liver Surgery, State Key Laboratory of Complex Severe and Rare Diseases, Peking Union Medical College Hospital, Chinese Academy of Medical Sciences, Peking Union Medical College, No.1 Shuaifuyuan, Beijing 100730, China
[3]Eight-year Medical Doctor Program, Chinese Academy of Medical Sciences and Peking Union Medical College, Beijing, China

Received: 28 July 2024 / Accepted: 4 May 2025
Published online: 16 May 2025

References

1. Conroy M, Naidoo J. Immune-related adverse events and the balancing act of immunotherapy. Nat Commun. 2022;13(1):392.
2. Thuny F, Naidoo J, Neilan TG. Cardiovascular complications of immune checkpoint inhibitors for cancer. Eur Heart J. 2022;43(42):4458–68.
3. Heinzerling L, Ott PA, Hodi FS, Husain AN, Tajmir-Riahi A, Tawbi H, et al. Cardiotoxicity associated with CTLA4 and PD1 blocking immunotherapy. J Immunother Cancer. 2016;4:50.
4. Lehmann LH, Cautela J, Palaskas N, Baik AH, Meijers WC, Allenbach Y, et al. Clinical strategy for the diagnosis and treatment of immune checkpoint Inhibitor-Associated myocarditis: A narrative review. JAMA Cardiol. 2021;6(11):1329–37.
5. Basso C, Myocarditis. N Engl J Med. 2022;387(16):1488–500.
6. Zhu H, Galdos FX, Lee D, Waliany S, Huang YV, Ryan J, et al. Identification of pathogenic immune cell subsets associated with checkpoint Inhibitor-Induced myocarditis. Circulation. 2022;146(4):316–35.
7. Axelrod ML, Meijers WC, Screever EM, Qin J, Carroll MG, Sun X, et al. T cells specific for alpha-myosin drive immunotherapy-related myocarditis. Nature. 2022;611(7937):818–26.
8. Ma P, Liu J, Qin J, Lai L, Heo GS, Luehmann H, et al. Expansion of pathogenic cardiac macrophages in immune checkpoint inhibitor myocarditis. Circulation. 2024;149(1):48–66.
9. Litvinukova M, Talavera-Lopez C, Maatz H, Reichart D, Worth CL, Lindberg EL, et al. Cells of the adult human heart. Nature. 2020;588(7838):466–72.
10. Hao Y, Hao S, Andersen-Nissen E, Mauck WM 3rd, Zheng S, Butler A, et al. Integrated analysis of multimodal single-cell data. Cell. 2021;184(13):3573–e8729.
11. Wolock SL, Lopez R, Klein AM, Scrublet. Computational identification of cell doublets in Single-Cell transcriptomic data. Cell Syst. 2019;8(4):281–91. e9.
12. Yang S, Corbett SE, Koga Y, Wang Z, Johnson WE, Yajima M et al. Decontamination of ambient RNA in single-cell RNA-seq with decontx. Genome Biol. 2020;21(1).
13. Korsunsky I, Millard N, Fan J, Slowikowski K, Zhang F, Wei K, et al. Fast, sensitive and accurate integration of single-cell data with harmony. Nat Methods. 2019;16(12):1289–96.
14. Zappia L, Oshlack A. Clustering trees: a visualization for evaluating clusterings at multiple resolutions. Gigascience. 2018;7(7):giy083.
15. Davis FM, Tsoi LC, Ma F, Wasikowski R, Moore BB, Kunkel SL, et al. Single-cell transcriptomics reveals dynamic role of smooth muscle cells and enrichment of immune cell subsets in human abdominal aortic aneurysms. Ann Surg. 2022;276(3):511–21.
16. Tuschl T, Buyon JP, Halushka MK, Morozov P, Clancy R, Suryawanshi H. Cell atlas of the foetal human heart and implications for autoimmune-mediated congenital heart block. Cardiovasc Res. 2020;116(8):1446–57.
17. Hill MC, Kadow ZA, Long H, Morikawa Y, Martin TJ, Birks EJ, et al. Integrated multi-omic characterization of congenital heart disease. Nature. 2022;608(7921):181–91.
18. Gonzalez H, Mei W, Robles I, Hagerling C, Allen BM, Hauge Okholm TL, et al. Cellular architecture of human brain metastases. Cell. 2022;185(4):729–45. e20.
19. Koenig AL, Shchukina I, Amrute J, Andhey PS, Zaitsev K, Lai L, et al. Single-cell transcriptomics reveals cell-type-specific diversification in human heart failure. Nat Cardiovasc Res. 2022;1(3):263–80.
20. Jung C, Han JW, Lee SJ, Kim KH, Oh JE, Bae S et al. Novel directly reprogrammed smooth muscle cells promote vascular regeneration as microvascular mural cells. Circulation. 2025;151(15):1076–94.
21. de Rooij LPMH, Becker LM, Teuwen L-A, Boeckx B, Jansen S, Feys S, et al. The pulmonary vasculature in lethal COVID-19 and idiopathic pulmonary fibrosis at single-cell resolution. Cardiovasc Res. 2023;119(2):520–35.
22. Yousef H, Czupalla CJ, Lee D, Chen MB, Burke AN, Zera KA, et al. Aged blood impairs hippocampal neural precursor activity and activates microglia via brain endothelial cell VCAM1. Nat Med. 2019;25(6):988–1000.
23. Barnett SN, Cujba A-M, Yang L, Maceiras AR, Li S, Kedlian VR, et al. An organotypic atlas of human vascular cells. Nat Med. 2024;30(12):3468–81.
24. Wu T, Hu E, Xu S, Chen M, Guo P, Dai Z, et al. ClusterProfiler 4.0: A universal enrichment tool for interpreting omics data. Innov. 2021;2(3):100141.
25. Hanzelmann S, Castelo R, Guinney J. GSVA: gene set variation analysis for microarray and RNA-seq data. BMC Bioinformatics. 2013;14:7.
26. Chung W, Eum HH, Lee HO, Lee KM, Lee HB, Kim KT, et al. Single-cell RNA-seq enables comprehensive tumour and immune cell profiling in primary breast cancer. Nat Commun. 2017;8(1):15081.
27. Liu B, Hu X, Feng K, Gao R, Xue Z, Zhang S, et al. Temporal single-cell tracing reveals clonal revival and expansion of precursor exhausted T cells during anti-PD-1 therapy in lung cancer. Nat Cancer. 2022;3(1):108–21.
28. Gaude E, Frezza C. Tissue-specific and convergent metabolic transformation of cancer correlates with metastatic potential and patient survival. Nat Commun. 2016;7(1):13041.

29. Liu C, Yu H, Huang R, Lei T, Li X, Liu M, et al. Radioimmunotherapy-induced intratumoral changes in cervical squamous cell carcinoma at single-cell resolution. Cancer Commun. 2022;42(12):1407–11.
30. Sun Y, Wu L, Zhong Y, Zhou K, Hou Y, Wang Z, et al. Single-cell landscape of the ecosystem in early-relapse hepatocellular carcinoma. Cell. 2021;184(2):404–21. e16.
31. Cao J, Spielmann M, Qiu X, Huang X, Ibrahim DM, Hill AJ, et al. The single-cell transcriptional landscape of mammalian organogenesis. Nature. 2019;566(7745):496–502.
32. Qiu X, Hill A, Packer J, Lin D, Ma YA, Trapnell C. Single-cell mRNA quantification and differential analysis with census. Nat Methods. 2017;14(3):309–15.
33. Jin S, Guerrero-Juarez CF, Zhang L, Chang I, Ramos R, Kuan CH, et al. Inference and analysis of cell-cell communication using cellchat. Nat Commun. 2021;12(1):1088.
34. Badia IMP, Velez Santiago J, Braunger J, Geiss C, Dimitrov D, Muller-Dott S, et al. DecoupleR: ensemble of computational methods to infer biological activities from omics data. Bioinform Adv. 2022;2(1):vbac016.
35. Jiang P, Zhang Y, Ru B, Yang Y, Vu T, Paul R, et al. Systematic investigation of cytokine signaling activity at the tissue and single-cell levels. Nat Methods. 2021;18(10):1181–91.
36. Lasrado N, Borcherding N, Arumugam R, Starr TK, Reddy J. Dissecting the cellular landscape and transcriptome network in viral myocarditis by single-cell RNA sequencing. iScience. 2022;25(3).
37. Mantri M, Hinchman MM, McKellar DW, Wang MFZ, Cross ST, Parker JSL, et al. Spatiotemporal transcriptomics reveals pathogenesis of viral myocarditis. Nat Cardiovasc Res. 2022;1(10):946–60.
38. Hua X, Hu G, Hu Q, Chang Y, Hu Y, Gao L, et al. Single-Cell RNA sequencing to dissect the immunological network of autoimmune myocarditis. Circulation. 2020;142(4):384–400.
39. Butler A, Hoffman P, Smibert P, Papalexi E, Satija R. Integrating single-cell transcriptomic data across different conditions, technologies, and species. Nat Biotechnol. 2018;36(5):411–20.
40. Zhang L, Yu X, Zheng L, Zhang Y, Li Y, Fang Q, et al. Lineage tracking reveals dynamic relationships of T cells in colorectal cancer. Nature. 2018;564(7735):268–72.
41. Miranda AMA, Janbandhu V, Maatz H, Kanemaru K, Cranley J, Teichmann SA, et al. Single-cell transcriptomics for the assessment of cardiac disease. Nat Rev Cardiol. 2023;20(5):289–308.
42. Matzen E, Bartels LE, Logstrup B, Horskaer S, Stilling C, Donskov F. Immune checkpoint inhibitor-induced myocarditis in cancer patients: a case report and review of reported cases. Cardiooncology. 2021;7(1):27.
43. Zhang Q, He Y, Luo N, Patel SJ, Han Y, Gao R, et al. Landscape and dynamics of single immune cells in hepatocellular carcinoma. Cell. 2019;179(4):829–45. e20.
44. Gaber T, Strehl C, Buttgereit F. Metabolic regulation of inflammation. Nat Rev Rheumatol. 2017;13(5):267–79.
45. Wright RD, Cooper D. Glycobiology of leukocyte trafficking in inflammation. Glycobiology. 2014;24(12):1242–51.
46. Nolz JC, Harty JT. IL-15 regulates memory CD8 + T cell O-glycan synthesis and affects trafficking. J Clin Invest. 2014;124(3):1013–26.
47. Shi S, Gu S, Han T, Zhang W, Huang L, Li Z, et al. Inhibition of MAN2A1 enhances the immune response to Anti-PD-L1 in human tumors. Clin Cancer Res. 2020;26(22):5990–6002.
48. Zernecke A, Erhard F, Weinberger T, Schulz C, Ley K, Saliba AE, et al. Integrated single-cell analysis-based classification of vascular mononuclear phagocytes in mouse and human atherosclerosis. Cardiovasc Res. 2023;119(8):1676–89.
49. Domanska D, Majid U, Karlsen VT, Merok MA, Beitnes AR, Yaqub S, et al. Single-cell transcriptomic analysis of human colonic macrophages reveals niche-specific subsets. J Exp Med. 2022;219(3):e20211846.
50. Liu Y, Xu R, Gu H, Zhang E, Qu J, Cao W, et al. Metabolic reprogramming in macrophage responses. Biomark Res. 2021;9(1):1.
51. Bosca L, Gonzalez-Ramos S, Prieto P, Fernandez-Velasco M, Mojena M, Martin-Sanz P, et al. Metabolic signatures linked to macrophage polarization: from glucose metabolism to oxidative phosphorylation. Biochem Soc Trans. 2015;43(4):740–4.
52. Chen P, Wang Y, Li J, Bo X, Wang J, Nan L, et al. Diversity and intratumoral heterogeneity in human gallbladder cancer progression revealed by single-cell RNA sequencing. Clin Transl Med. 2021;11(6):e462.
53. Banerjee S, Biehl A, Gadina M, Hasni S, Schwartz DM. JAK-STAT signaling as a target for inflammatory and autoimmune diseases: current and future prospects. Drugs. 2017;77(5):521–46.
54. Najm A, Masson FM, Preuss P, Georges S, Ory B, Quillard T, et al. MicroRNA-17-5p reduces inflammation and bone erosions in mice with Collagen-Induced arthritis and directly targets the JAK/STAT pathway in rheumatoid arthritis Fibroblast-like synoviocytes. Arthritis Rheumatol. 2020;72(12):2030–9.
55. Reith W, LeibundGut-Landmann S, Waldburger JM. Regulation of MHC class II gene expression by the class II transactivator. Nat Rev Immunol. 2005;5(10):793–806.
56. Handunnetthi L, Ramagopalan SV, Ebers GC, Knight JC. Regulation of major histocompatibility complex class II gene expression, genetic variation and disease. Genes Immun. 2010;11(2):99–112.
57. Bonelli M, Dalwigk K, Platzer A, Olmos Calvo I, Hayer S, Niederreiter B, et al. IRF1 is critical for the TNF-driven interferon response in rheumatoid fibroblast-like synoviocytes: JAKinibs suppress the interferon response in RA-FLSs. Exp Mol Med. 2019;51(7):1–11.
58. Yang P, Manaenko A, Xu F, Miao L, Wang G, Hu X, et al. Role of PDGF-D and PDGFR-β in neuroinflammation in experimental ICH mice model. Exp Neurol. 2016;283(Pt A):157–64.
59. Nibbs RJ, Graham GJ. Immune regulation by atypical chemokine receptors. Nat Rev Immunol. 2013;13(11):815–29.
60. Collier JL, Pauken KE, Lee CAA, Patterson DG, Markson SC, Conway TS, et al. Single-cell profiling reveals unique features of diabetogenic T cells in anti-PD-1-induced type 1 diabetes mice. J Exp Med. 2023;220(10):e20221920.
61. Sun L, Yang X, Yuan Z, Wang H. Metabolic reprogramming in immune response and tissue inflammation. Arterioscler Thromb Vasc Biol. 2020;40(9):1990–2001.
62. Kim EY, Teh HS. Critical role of TNF receptor type-2 (p75) as a costimulator for IL-2 induction and T cell survival: a functional link to CD28. J Immunol. 2004;173(7):4500–9.
63. Alam MS, Otsuka S, Wong N, Abbasi A, Gaida MM, Fan Y, et al. TNF plays a crucial role in inflammation by signaling via T cell TNFR2. Proc Natl Acad Sci U S A. 2021;118(50):e2109972118.
64. Zhang QY, Ye XP, Zhou Z, Zhu CF, Li R, Fang Y, et al. Lymphocyte infiltration and thyrocyte destruction are driven by stromal and immune cell components in Hashimoto's thyroiditis. Nat Commun. 2022;13(1):775.
65. Kaufmann M, Schaupp AL, Sun R, Coscia F, Dendrou CA, Cortes A, et al. Identification of early neurodegenerative pathways in progressive multiple sclerosis. Nat Neurosci. 2022;25(7):944–55.
66. Su F, Zhang W, Meng L, Zhang W, Liu X, Liu X, et al. Multimodal Single-Cell analyses outline the immune microenvironment and therapeutic effectors of interstitial cystitis/bladder pain syndrome. Adv Sci. 2022;9(18):e2106063.
67. Reynolds G, Vegh P, Fletcher J, Poyner EFM, Stephenson E, Goh I, et al. Developmental cell programs are co-opted in inflammatory skin disease. Science. 2021;371(6527):eaba6500.
68. Korsunsky I, Wei K, Pohin M, Kim EY, Barone F, Major T, et al. Cross-tissue, single-cell stromal atlas identifies shared pathological fibroblast phenotypes in four chronic inflammatory diseases. Med. 2022;3(7):481–e51814.
69. Liu Q, Yu Y, Lin J, Wang Y, Ai L, Li Q, et al. Treatment strategy for myocarditis in patients using immune checkpoint inhibitors or combined anti-vascular endothelial growth factor therapy by clinical severity. Eur J Cancer. 2021;157:10–20.
70. Zhang L, Awadalla M, Mahmood SS, Nohria A, Hassan MZO, Thuny F, et al. Cardiovascular magnetic resonance in immune checkpoint inhibitor-associated myocarditis. Eur Heart J. 2020;41(18):1733–43.
71. Tan WLW, Seow WQ, Zhang A, Rhee S, Wong WH, Greenleaf WJ, et al. Current and future perspectives of single-cell multi-omics technologies in cardiovascular research. Nat Cardiovasc Res. 2023;2(1):20–34.

Publisher's note